University of Southern Queensland

Faculty of Engineering and Surveying

NUMERICAL MODELLING OF HORIZONTAL FLOW IN SAND FILTERS

A dissertation submitted by

Stuart Mead

In fulfillment of the requirements of

Courses ENG4111 and ENG4112 Research Project

towards the degree of

Bachelor of Engineering/Business

(Mechanical/Logistics and Operations Management)

29 October 2009

Abstract

This research investigates the option of using horizontal sand filters for water filtration to replace the currently used vertical filters. This project carries out the investigation using computational fluid dynamics (CFD) software to develop an optimal configuration for a horizontal sand filter using baffles in the geometry to disrupt the flow.

Saturated sand consolidates to 95% of its unsaturated volume and creates a channel in the top of a horizontally laid sand filter, which the majority of the water flows through due to Darcy's law. Previous research on the topic has determined that the addition of baffles to disrupt the flow in the channeled area reduces this effect.

The development of an optimum configuration was done using CFD software, and the findings were validated using experimental data. The numerical modeling results show that the optimal baffle spacing in the case of a 0.2m diameter pipe, for inlet velocities of between 0.002 and 0.01 m/s is 4.5cm with a baffle depth of 0.05m. More importantly it has been found that a relationship between the velocity profile and the baffle spacing exists which allows for filter designs to be optimised based on targeted filtration effectiveness.

University of Southern Queensland
Faculty of Engineering and Surveying

ENG4111 Research Project Part 1 &
ENG4112 Research Project Part 2

Limitations of Use

The Council of the University of Southern Queensland, its Faculty of Engineering and Surveying, and the staff of the University of Southern Queensland, do not accept any responsibility for the truth, accuracy or completeness of material contained within or associated with this dissertation.

Persons using all or any part of this material do so at their own risk, and not at the risk of the Council of the University of Southern Queensland, its Faculty of Engineering and Surveying or the staff of the University of Southern Queensland.

This dissertation reports an educational exercise and has no purpose or validity beyond this exercise. The sole purpose of the course "Project and Dissertation" is to contribute to the overall education within the student's chosen degree programme. This document, the associated hardware, software, drawings, and other material set out in the associated appendices should not be used for any other purpose: if they are so used, it is entirely at the risk of the user.

Professor Frank Bullen
Dean
Faculty of Engineering and Surveying

Certification

I certify that the idea, designs and experimental work, results, analyses and conclusions set out in this dissertation are entirely my own effort, except where otherwise indicated and acknowledged.

I further certify that this work is original and has not been previously submitted for assessment in any other course or institution, except where specifically stated.

Stuart Mead

Student Number: 0050041389

Signature: _____

Date: _____

Acknowledgements

I would like to thank my supervisors Dr. Ruth Mossad and Dr. Hal Aral for their valuable contributions towards this project. Their enthusiasm, support and direction throughout the year has enabled me to accomplish all the goals I have set out to achieve in this research project. Particular thanks go to Dr. Hal Aral and CSIRO Minerals, Clayton whose financial support allowed me to undertake the experimental validation which has proved extremely valuable.

Table of Contents

List of Figures

List of Tables

Nomenclature

A	Cross-sectional Area
C_w	A porous media constant used to determine flow regimes
D	Pipe diameter
D_{exp}	Generic Measured Value
D_p	Hydraulic diameter of porous medium
$d_{p.e,s}$	Effective sand diameter
E_Q	Generic Quantifiable Error Value
e_s	Suspended particle size
E_{UQ}	Generic Unquantifiable Error Value
$g_{x,y,z}$	Gravity
h	Height of Water
i	Filtration coefficient
k & α	Permeability
L	Length of filter medium
n	Porous media thickness
P & p	Pressure
p_E	Pressure Error
Q	Flow Rate
Re	Superficial Reynolds Number
Re_k	Reynolds number based on permeability
Re_p	Reynolds number within the pores of the medium
RUC	Representative Unit Cell
S	Generic Simulation Value
$S_{x,y,z}$	Source term representing the pressure gradient due to the effect of the porous media
u	Velocity in the x direction
U	Uncertainty Percentage
U_c	Non Uniformity Coefficient
v	Velocity in the y direction
V_D	Measured velocity
V_{FE}	Velocity error due to the flowmeter
V_p	Velocity within the pores
V_s	Superficial Velocity
V_S	Simulated velocity
w	Velocity in the x direction
ε	Porosity of the sand
P	Fluid Density
μ	Dynamic Viscosity

Chapter 1-Introduction

1.1-Outline

This research investigates and further develops the concept of using horizontal sand filters for water filtration identified by Mossad and Aral (2009). The issue with standard vertical sand filters is that there is a practical limit to the depth of the filter medium. A horizontal filter offers the advantage of being used for in-line filtration as well as having less constraints of the length of the filter medium; however they are currently not used because the settlement of the wet sand creates a least resistance channel at the top, which the majority of the fluid follows. This project investigates, using computational fluid dynamics software, an optimal configuration for a horizontal sand filter using baffles in the geometry to encourage the flow downward through the sand filter.

1.2-Introduction

In a typical water treatment plant, filtration has usually been regarded as the most important step in providing potable water. This step significantly enhances the quality of the water by removing most suspended particles and bacteria present in the water, making it almost potable (Binnie, 2002). In a sand filter's typical vertical configuration, water is pumped to the top of the filter and fed down through the sand using gravity.

In order to achieve the desired flow rates, there needs to be a sufficient pressure gradient as defined by Darcy's law (Darcy, 1856). This pressure is either achieved through pressurization or through raising the water level above the filter medium, using gravity to full advantage. Typically, in vertical filters the water is fed through the medium through gravity. This means

that as the filter medium gets taller, the supernatant[1] water level has to increase too; making vertical filters impractical above certain filter depths.

Additionally, significant headloss occurs in the collection mechanism of vertical filters due to the fact that it needs to provide the structure to hold up the filter medium as well as collecting the fluid. Figure 1.2.1 shows the collection device used in the Tugun desalination plant on the Gold Coast, Australia. A horizontal filter does not have to have such a bulky structure to collect the filtered water because it is not bearing the weight of the sand, instead a simple screen would suffice; allowing for easier in line treatment of water.

Figure 1.2.1-Sand Filter Collection Mechanism

This disadvantage, combined with the demand for longer, more effective sand filters for use in advanced technologies such as reverse osmosis (American Water Works Association, 2007) means that solutions need to be found to reduce the headloss that happens in the filtration stage. Currently, there are no viable alternatives for high volume filtration that reduce the headloss.

[1] The water above the sand filter

1.3-Background

This project follows on from the work of Mossad and Aral (2009) who initially identified the possibility of using horizontal filters. The sand was seen to compact to 95% of its original volume which created a path of least resistance at the top of the pipe. Several different geometries were analysed to find a suitable solution to reducing the flow in the channelled area. From this investigation, three geometries were identified for further research; these were a spiral protrusion through the pipe, baffles at the top of the pipe and a pipe with a downpipe attached.

From these three geometries, it was decided to optimise the solution for the baffled geometry; the effect depth, width, shape and spacing has on the flow will be analysed in order to achieve a solution that minimises the effect of the channelling at the top of the pipe. This geometry was chosen due to its design simplicity which would make manufacturing of industrial models viable and the fact that it showed the most promise to achieve an optimal solution that would eliminate the effect of the low resistance channel.

Further research into this area will provide an optimal configuration for a horizontally laid sand filter which could be a viable alternative to current sand filtration methods.

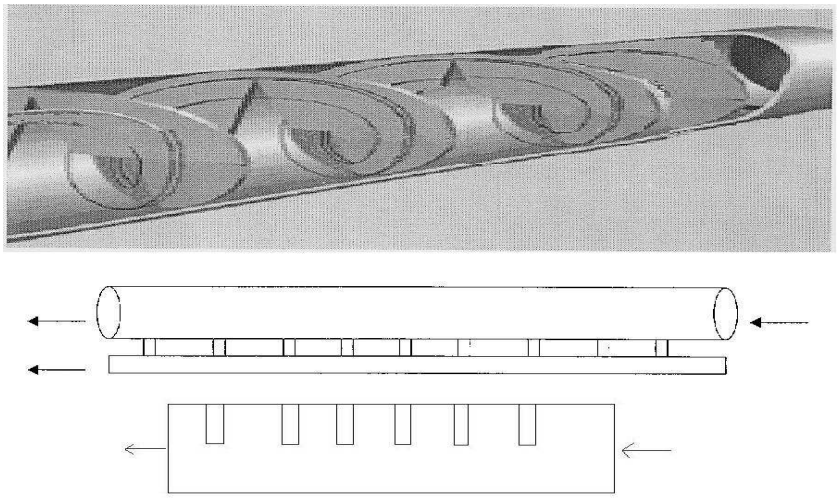

Figure 1.3.1-Three alternate geometries identified by Mossad and Aral (2009)

1.4-Objectives

The objective of this project is to develop an optimum configuration for a horizontally laid sand filter that will reduce the effect of the channelling that occurs. Consideration will be given to the end use of the filter in order to ensure its viability in terms of headloss, flow rates and filtration efficiency.

The horizontal column's baffled geometry size, shape and position will be modified so that water sweeps through the filter medium rather than the channelled section. Other methods of altering the flow profile such as altering the properties of the medium and flow rates will be investigated once an optimum geometry is found to derive a relationship for determining the optimal configuration.

This optimum geometrical configuration will then be tested in laboratory experiments to determine the validity of the results and to investigate any other phenomena that may have been neglected in the CFD analysis. This laboratory setup will also prove valuable for any future work on the topic such as investigating backwash methods or the filtration efficiency of the filter.

Chapter 2-Background Information

2.1-Outline

This chapter will investigate the relevant areas of importance for the analysis of this flow problem. The main area of investigation is in the field of fluid transport through and within saturated porous media, this covers aspects such as geometric properties of porous media, equations for flow across porous media and fluid dynamics considerations arising from the Reynolds number of the flow. The second area of investigation is current filtration methods and applications, with consideration of the key objectives in sand filtration, sand filter design and advances in lateral flow sand filter design.

2.2-Porous Media Transport

2.2.1-Important geometric properties of porous media

Definition

The term 'porous media' encompasses a wide variety of materials, of varying sizes, material types and shapes. A few examples of porous media include sand, grain, cloth and the rows of pipes present in heat exchangers. The many different substances that fit into the porous media category mean that the media needs to be arranged into classes according to their pore spaces. Pore spaces can be classed by their hydrodynamic effects as voids, capillaries or force spaces, and are divided into ordered or disordered pore spaces which can also be either dispersed or connected. (Schiedegger 1960) Filtration sand is classed as a capillary since the walls of the sand have a significant effect on the hydrodynamics of the flow and generally has connected but disordered pore spaces.

Porosity

The porosity of a porous medium is described as the fraction of void to total volume and is expressed as either a percentage or fraction of 1(Schiedegger 1960). FLUENT™ solvers assume that the pores of a porous medium are 100% open[2] (FLUENT™ User Guide), meaning that all the voids are interconnected. This definition of porosity is called the *effective porosity* and is calculated by only using the interconnected void spaces. Typical effective porosity values for filtration sand is in the range of 0.4 to 0.5 (Natare Corporation, 2003, Ward, 1964, Kawamura, 2000, Binnie et. Al 2002).

Effective Diameter

The effective size of sand is defined as the 10 percentile size (90% bigger, 10% smaller) of the sample and the variation in effective diameter is measured by the non uniformity coefficient, defined as:

$$U_c = \frac{60\ percentile\ size}{effective\ size}$$

Experimental analysis shows that the hydraulic characteristics of a filter bed such as flowrates and headloss are the same up to a non-uniformity coefficient of 2.08 (Natare Corporation, 2003).

The effective grain diameter of the porous medium is closely related to permeability; which is a term used to describe the resistance to flow of a porous medium. The effective diameter is used to determine permeability in calculations by Ward (1964), Vafai (2000) and du Plessis & Diedericks (1997). While these authors have experimentally proven the validity of their respective formula's to be an accurate description of permeability, Shciedegger (1960) concludes that grain size and grain size distribution has no meaningful relationship with the pore spaces and therefore permeability. Nonetheless, filtration sand is specified by effective diameter and is important for theoretical calculations of permeability.

[2] Meaning that all the spaces are interconnected

Filtration sand has an effective diameter of 0.45 to 1 mm with a non-uniformity coefficient of 1.6. (Binnie et. Al, 2002, Natare Corporation, 2003)

The Representative Unit Cell

du Plessis and Diedericks (1997) created a model to determine the interstitial flow conditions of porous media. The porosity, effective diameter and general properties discussed above are all based on a volume large enough to get a statistical average, the representative unit cell (RUC) is an elementary control volume consisting of a particle and the pore space.

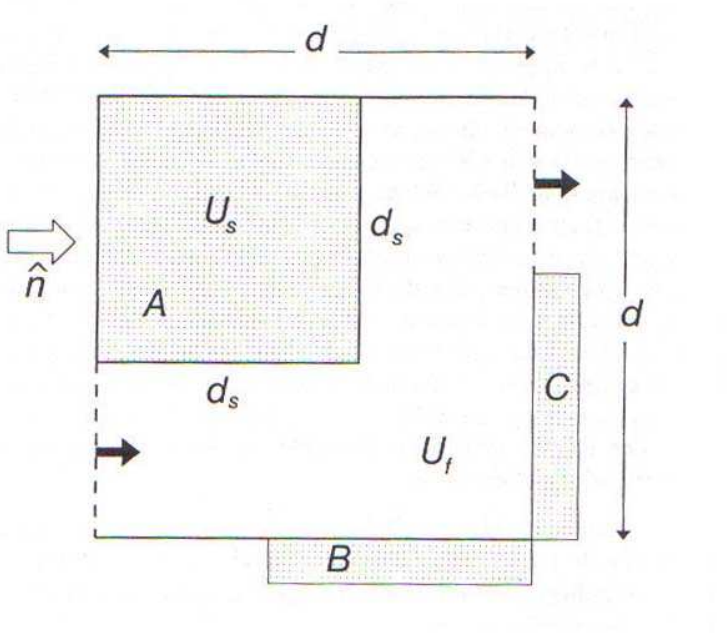

Figure 2.2.1-The RUC (du Plessis 1997)

In an isotropic, homogenous medium the RUC simplifies to the above diagram for a 2 dimensional problem. The volume U_s is a fraction of the RUC relative to its porosity and the effective diameter d_s is the same as the calculated effective diameter. B and C are other RUC's bordering to cell A, and an elemental solution for the velocity between the pores should be able to be calculated. This method is essentially how FLUENT™ determines the physical velocity between the pores.

2.2.2-Flow equations for porous media

The fundamental equation for flow through porous media is Darcy's law; it is a linear law similar in form to other popular linear relationships such as Ohm's and Fourier's law (Freeze, 1994). Darcy (1856) states that "…for identical sands, one can assume that the discharge is directly proportional to the head and inversely proportional to the thickness of the layer transversed." The law can be expressed in equation form as (Darcy 1856):

$$Q = kA\frac{h_1 - h_2}{L}$$

From visual inspection of the formula it can be converted into an expression relating the pressure difference to flow rate:

$$Q = \frac{-kA}{\mu}\frac{P_2 - P_1}{L}$$

Darcy's experiment can be replicated in any orientation and is commonly used to experimentally determine permeability values.

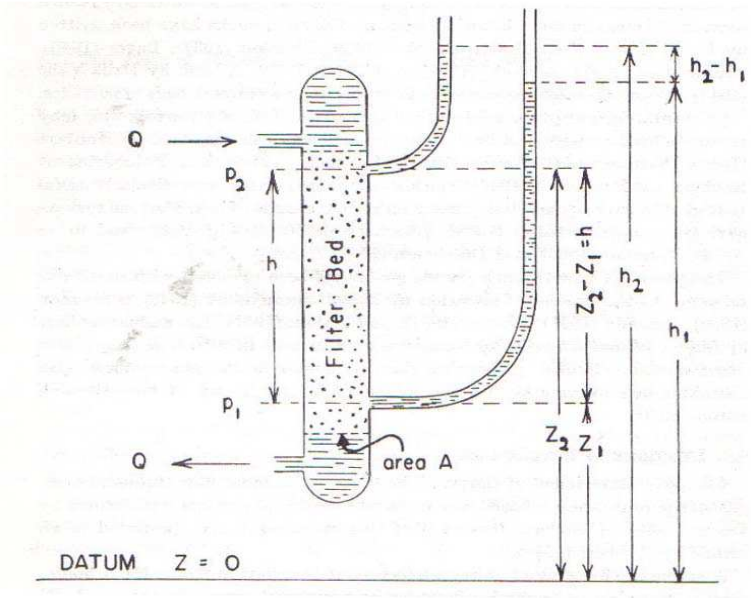

Figure 2.2.2 -A simple diagram of Darcy's Experiment (Shciedegger, 1960)

The flow is governed by the continuity and Navier-Stokes (momentum) and continuity equations which FLUENT™ solves. In this case the flow assumed to be steady, incompressible, laminar and Newtonian. Therefore the governing equations can then be simplified to:

$$\frac{\partial u}{\partial x}+\frac{\partial v}{\partial y}+\frac{\partial w}{\partial z}=0$$

$$\rho\left(u\frac{\partial u}{\partial x}+v\frac{\partial u}{\partial y}+w\frac{\partial u}{\partial z}\right)=\rho g_x-\frac{\partial p}{\partial x}+\mu\left(\frac{\partial^2 u}{\partial x^2}+\frac{\partial^2 u}{\partial y^2}+\frac{\partial^2 u}{\partial z^2}\right)+S_x$$

$$\rho\left(u\frac{\partial v}{\partial x}+v\frac{\partial v}{\partial y}+w\frac{\partial v}{\partial z}\right)=\rho g_y-\frac{\partial p}{\partial x}+\mu\left(\frac{\partial^2 v}{\partial x^2}+\frac{\partial^2 v}{\partial y^2}+\frac{\partial^2 v}{\partial z^2}\right)+S_y$$

$$\rho\left(u\frac{\partial w}{\partial x}+v\frac{\partial w}{\partial y}+w\frac{\partial w}{\partial z}\right)=\rho g_z-\frac{\partial p}{\partial x}+\mu\left(\frac{\partial^2 w}{\partial x^2}+\frac{\partial^2 w}{\partial y^2}+\frac{\partial^2 w}{\partial z^2}\right)+S_z$$

(FLUENT™ User Guide & Fox et. al 2009)

Where $S_{x,y,z}$ are source terms which contribute to the pressure gradient in the cell, in the case of a homogenous porous medium in laminar flow the scource term is:

$$S_i=-(\frac{\mu}{\alpha}v_i)$$

Or

$$\nabla p=-\frac{\mu}{\alpha}\vec{v}$$

Which is almost identical to the pressure gradient Vafai (2000) derived from Darcy's Law as:

$$-\nabla P=\frac{\mu V_s}{k}$$

Darcy's law has a few limitations as to its use; first it is assumed that the porous media is an isotropic homogenous medium and the second is that the law is only valid for very low Reynolds numbers, at higher velocities an extra term must be added to Darcy's momentum equation to account for the inertial effects.

Venkataraman & Rao (1998) have investigated and determined the cut off points for Darcy, non-linear and fully turbulent flow in porous media.

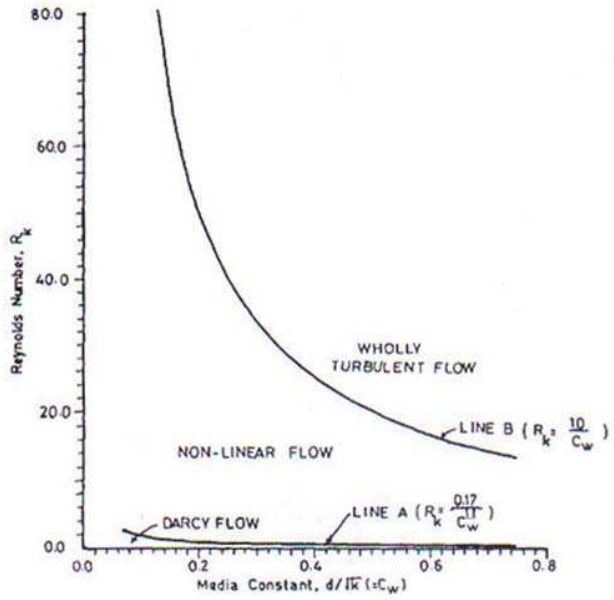

Figure 2.2.3-Delineation of Darcy, Nonlinear, and Turbulent Flows (Venkataraman & Rao 1998)

The above diagram shows the cut off lines separating the different flow regimes, where the media constant C_w is described as:

$$C_w = \frac{d}{\sqrt{k}}$$

Venkataraman & Rao explain the flow regime in the non-linear area as being in two parts, the first half can be assumed as non-linear Darcy flow, and the second half assumed as non-linear turbulent flow. Ward (1964) developed a relationship between the dimensionless fanning

factor and Reynolds number for porous media that is valid for both laminar and turbulent flows from which an equation valid for laminar and turbulent flow can be defined:

$$\frac{dp}{dl} = \frac{\mu V_s}{k} + \frac{0.55 \rho V_s^2}{k^{1/2}}$$

However, this equation is only valid for a particular media constant of 0.55 and would have to be redefined for other media constants if the need arises to analyse flow regimes other than pure Darcy flow.

2.2.3-Permeability of a Porous Medium

As can be seen through Darcy's law, the permeability of the medium is a very important dimension for calculating flow in porous structures. Permeability has the dimension of *Length*^{2} and is a function of the properties of the fluid and the porous medium (Scheidegger, 1960). Several relationships have been developed to calculate the permeability of a medium from known quantities such as porosity and grain diameter which have been proven empirically, however it is important to note that these correlations between experimental and theoretical results do not prove causation between the input variables and permeability (Schiedegger, 1960). Nonetheless, these theoretical calculations can be used in models until testing is carried out on the actual permeability of the filtration sand.

Vafai (2000) described the relationship between permeability, porosity and effective diameter as being:

$$k = \frac{\epsilon^3 d_p^2}{a(1-\epsilon)^2}$$

This relationship was used by Mossad and Aral (2009) in previous work on this topic.

The FLUENT™ user guide (section 7.19-17) uses the same relationship and notes that the constant *a* is equal to 150. In the alternative RUC estimation developed by du Plessis & Diedericks the permeability is determined as

$$k = \frac{\epsilon d^2 \left(1 - (1-\epsilon)^{1/3}\right)\left(1 - (1-\epsilon)^{2/3}\right)}{36(1-\epsilon)^{2/3}}$$

However it is important to note that the value *d* in this equation is the microscopic characteristic length which is related to the particle effective diameter by the equation

$$d = \frac{d_s}{(1-\epsilon)^{1/3}}$$

(du Plessis & Diedericks, 1997).

Venkataraman & Rao (1998) collated experimental permeability data, along with effective diameter and porosity from Ward (1964) and Arbhabhirama & Dinoy (1973) which can be used to determine the accuracy of the theoretical calculations.

Reference				**Calculated Permeability (cm^2)**	
	Effective Diameter (cm)	**Porosity**	**Experimental Permeability (cm^2)**	**Vafai (2000)**	**du Plessis & Diedericks (1997)**
Ward (1964)	0.06	0.41	3.00E-06	4.99E-06	1.06E-04
Arbhabhirama & Dinoy (1973)	0.16	0.40	1.20E-05	3.00E-05	6.44E-04

Table 2.2.1-Experimental and theoretical permeability

As the above table shows, actual calculated values of permeability vary significantly from experimental determinations of permeability. This is mainly due to the experimental techniques and equipment used, since the shape, uniformity coefficient and level of isotropy are major factors for the determination of permeability that are very hard to control. For this reason, it is very important to experimentally confirm the permeability of filtration sand.

2.2.4-Reynolds number considerations

The Reynolds number is a dimensionless constant that is used to classify the flow regime in fluid problems, these flow regimes are laminar, transition and turbulent. In filtration, laminar flow is most common with turbulent flow being avoided mainly due to the high velocities and the negative effect this has on the filtration effectiveness. In its general form the Reynolds number is given by (Fox et. al 2009)

$$Re = \frac{\rho V_c L_c}{\mu}$$

where the velocity and length terms in the equation are defined as the 'characteristic' length and velocity of the fluid problem being studies. When considering a porous flow problem, there are some issues in determining the Reynolds number, mainly due to the fact that it is hard to determine what the characteristic units are. Binnie (2002) presents two equations for Reynolds number, the first being based on the superficial velocity through the medium:

$$Re = \frac{\rho D_p V_s}{\mu}$$

Binnie's second equation is based on the physical velocity between the particles of the medium and thus gives the Reynolds number of the flow between the porous medium:

$$Re_p = \frac{\rho D_p V_p}{(1-\epsilon)\mu}$$

du Plessis & Diedericks (1997) used the same formulation as Binnie for the overall Reynolds number, however defined the Reynolds number of the flow in the pores a little different:

$$Re_p = \frac{2}{1 + (1-\epsilon)^{2/3}} Re$$

Both of these Reynolds number formulations were defined with filtration sand being the media under consideration, whereas Ward (1964) created a more general equation for the Reynolds number in porous media as defined by:

$$Re_k = \frac{V_s k^{1/2} \rho}{\mu}$$

This is the Reynolds number that Venkataraman & Rao used to develop the cut off points to determine the flow regime in porous media and therefore it is important to determine the flow regime using this Reynolds number if using their work.

2.3-Filtration Methods and Applications

Binnie, Kimber and Smethurst (2002) state that the filtration stage has historically been considered the core of the process in traditional water treatment plants, where the quality of the water changes from clearly non-potable to almost drinkable water after the filtration process. A good quality filter should be able to produce filtered water with a turbidity [3] of less than 0.2 NTU which is lower than the general allowable standard of 0.3 NTU.

2.3.1-Filtration Theory

The filtration process has to remove particles that are far smaller than the sizes of the pores in the media, as Binnie et. al (2002) shows in the diagram below which identifies the main particles that need to be removed by filtration:

Material	Particle diameter (approx.) (μm)
Sand	800
Soil	1–100
Cryptosporidium oocysts	5
Bacteria	0.3–3
Viruses	0.005–0.01
Floc particles	100–2000

Figure 2.3.1-Relative size of sand grains and suspended matter (Binnie 2002)

As such, the filtration process is clearly more complex than simple straining. Horvath (1994) states six mechanisms for filtration, straining, interception, diffusion, inertia, settling and hydrodynamic action.

[3] The cloudiness of fluid caused by suspended solids

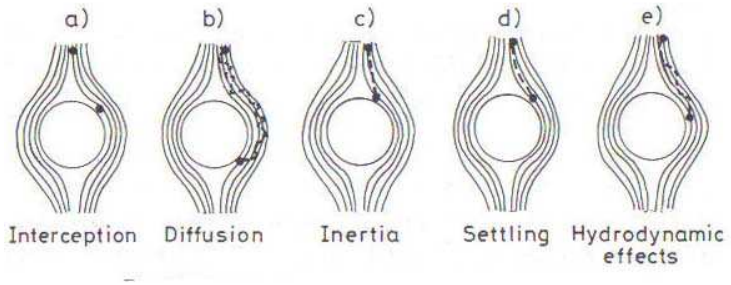

Figure 2.3.2 -Transport Mechanisms (Horvath 1994)

Straining

Straining is the least important filtration mechanism and the most undesirable one (Binnie 2002), this is due to the fact that the first layer of the filter bed will get clogged, making the filter very inefficient. For this reason, coagulation and flocculation pre-treatment are important processes that should occur prior to filtration.

Interception

Interception is the process by which suspended particles are directly intercepted by the filter particle and stays at that location due to adhesion. The interception occurs when a suspended particles flow line leads it to collide with the filter particles, the relationship that defines this phenomena is

$$i = \frac{e_s}{d_p}$$

from this relationship we can see that the larger suspended particles get filtered this way for a constant particle size. (Horvath, 1994)

Diffusion

Diffusion occurs due to the Brownian motion of the molecules in particles less than 1 millimicron in size. This causes the suspended particle to have a random flow path (Horvath, 1994). The number of collisions with filtration particles due to collisions is defined by Binnie (2002) as

$$i = \left(\frac{T}{d_p d_m V_p}\right)^{0.67}$$

and is only important at higher temperatures and for very small filtration and suspended particles.

Inertia

The inertial effect will cause heavier particles to deviate from their flow path when their streamlines curve around the particle and impact on the filtration particle. This effect is more significant in faster flow situations and is considered to be a minor factor in filtration mechanisms such as sand filters. (Binnie 2002)

Settling

Settling takes into account the gravitational forces of the suspended particles. Particle removal is relative to the ratio between the settling velocity and the velocity of the fluid, which is expressed in the relationship

$$i = \frac{g(\rho_s - \rho)e_s^2 / 18n}{V_p}$$

Hydrodynamic Action

The hydrodynamic effect of filtration comes about due to the suspended particles rotating because of the non-uniform velocity gradient present when passing between pores. The pressure difference caused by this rotation moves the particle towards the filtration particle. Due to the high velocities this action happens at it is viewed as negligible in sand filtration (Binnie 2002).

From this analysis of filtration mechanisms, the two 'controllable' inputs for filtration (V_p and D_p) are on the denominator, meaning that a lower velocity and lower particle diameter is desirable to get good filtration.

2.3.2-Sand Filter Design

The three most common types of sand filters in use at water treatment plants are slow sand filters, rapid sand filters and pressure filters (Kawamura, 2000). Slow sand filters are slowly being phased out in the industry and operate on a completely different principle from the filtration method being used in this study. Out of rapid sand filters and pressure filters, rapid sand filters are the most common and pressure filters are only usually used where the hydraulic conditions suit (Binnie 2002).

Rapid Sand Filters

Rapid sand filters and pressure filters operate on the same concept, however rapid sand filters use gravity to force the flow through the filter media whereas pressure filters use a pressurised system. Both types feed their water vertically through the media. The specifications of rapid sand filters vary according to the water treatment site layout and the specific needs of the treatment plant however typical specifications have been collated from various authors and are shown below.

	Rapid Sand Filter	**Pressure Filter**
Filtration Rate ($m^3/m^2/hr$)	5 to 15	
Filtration Velocity (m/hr)	5 to 7.5	
Filter Area (m^2)	1 to 4	
Bed Thickness (m)	0.6 to 3	
Sand grain size (mm)	0.4 to 0.65	0.4 to 0.65
Supernatant water level (m)	1 to 1.5	
Filtration Headloss (m)	1.5 to 4	7.5 to 15
Total Headloss (m)	2.7 to 4.5	15 to 30

Table 2.3.1 -Typical filter specifications (Kawamura, 2000. Rowe & Abdel-Magid, 1995)

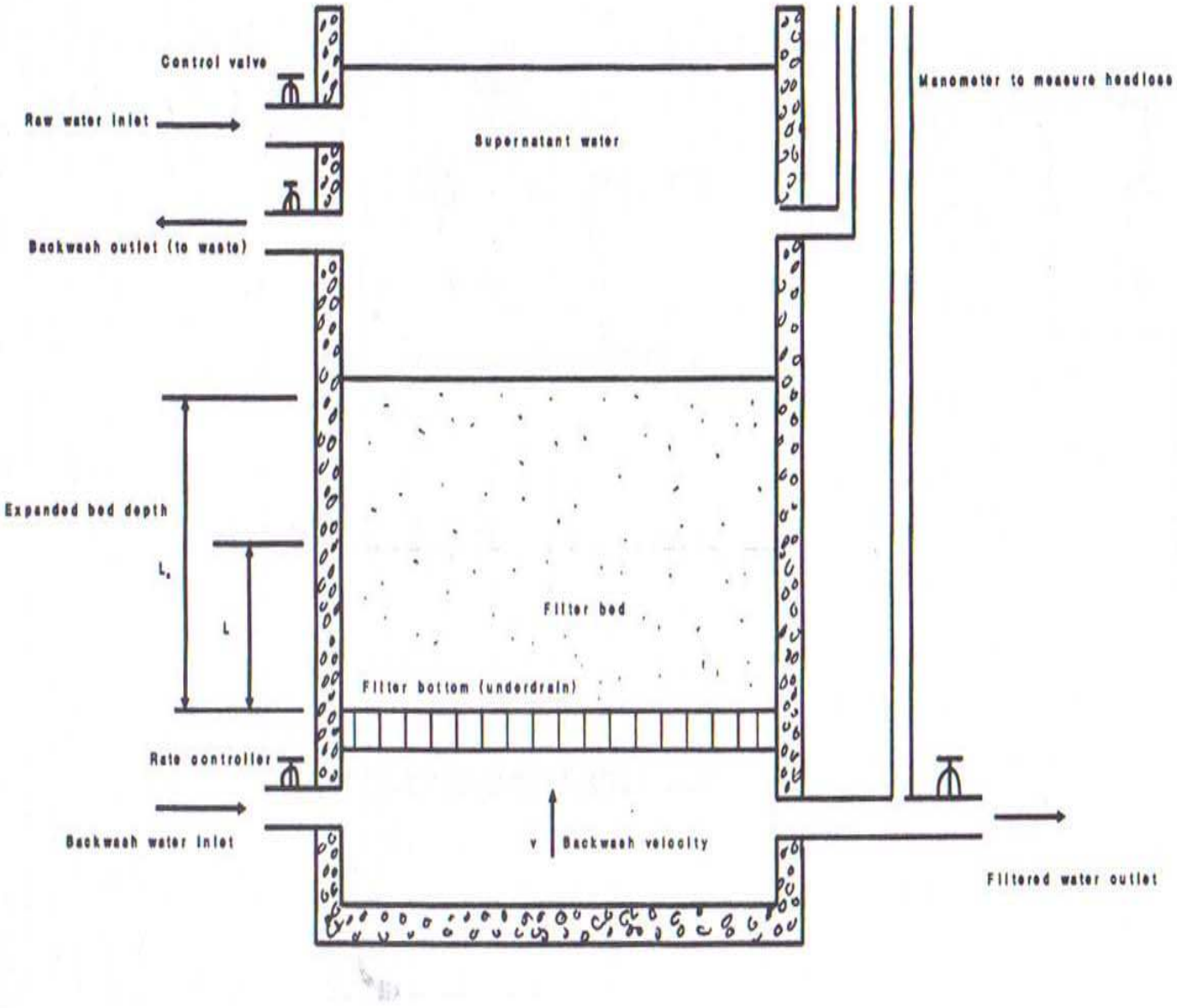

Figure 2.3.3 -Typical sand filter design (Rowe & Abdel-Magid, 1995)

Implications arising from Reverse Osmosis

Reverse osmosis (RO) is a relatively new technology in the field of wastewater management and uses membrane technology to treat the water to potable standards.

One of the requirements of RO systems is that the influent water has to be very clean, with the requirement that more than 99.9% of silt particles larger than 50µm be removed from the influent water, for this reason, RO pre-treatment filters are designed slightly differently to traditional sand filter systems, with a filtration velocity of less than 0.0027m/s (2-4 gpm/ft^2) and a deeper filter bed to remove more particles (American Water Works Association, 2007).

This requirement for slower velocities and deeper filter beds provide an opportunity for a horizontal type sand filter since they can be placed inline with the RO membranes unlike vertical filters.

Figure 2.3.2.4 & 2.3.2.5-Vertical Sand Filters and Reverse Osmosis Membranes at the Tugun Desalination Plant, Gold Coast, Australia. Horizontal filters provide the opportunity to provide inline filtration with the RO Membranes, greatly saving on space and infrastructure costs.

Lateral Flow Sand Filters

There has been little research into the use of lateral or horizontal flow sand filters, Havard et. al (2008) investigated the hydraulic performance of lateral flow sand filters based on a design investigated by Check (1994). However this system was mainly used to treat septic tank effluent and used a slightly sloping bed in order to move the flow laterally. Figure 2.3.2.2 below shows a diagram of the experimental setup used by Harvard et. al and shows how the problem of settlement of sand was solved.

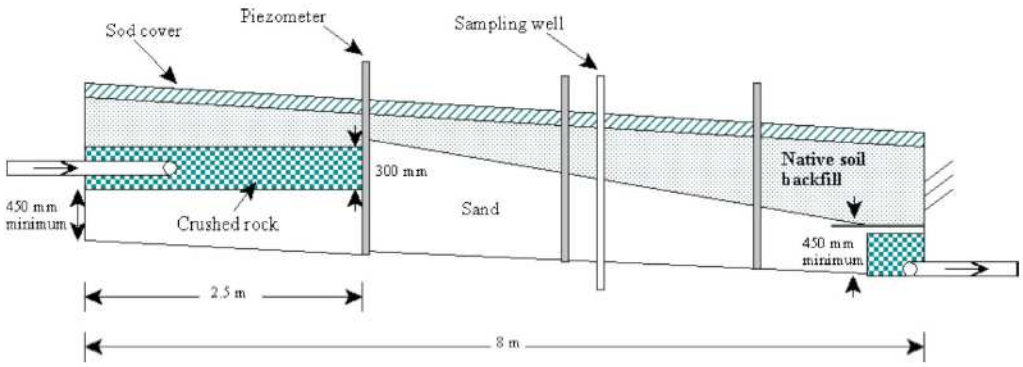

Figure 2.3.6-Harvard et. al's Lateral Flow Sand Filter (2008)

Firstly, the soil backfill would have eliminated any of the gaps that arose from the settlement of the sand and secondly the sand medium was unsaturated and the flow rates were very slow, meaning that gravity had a more significant effect than the resistance of the sand.

2.4-Summary

The properties of porous media, in particular permeability have a major effect on the flow through the porous media as shown by Darcy's law. The other significant factor that affects the flow through porous media is the Reynolds number, which denotes whether the flow is Darcian, transition or fully turbulent. There is significant variation in the theories of different authors (Ward, Vafai, du Plessis & Diedericks, Arbhabhirama & Dinoy) in the aspect of permeability which do not show any correlation to experimental results. Thus experimental results for permeability should be used if possible.

Current rapid filtration methods are able to handle large volumes of flow, however the headloss associated with vertical rapid sand filters is very high and any increase to the bed depth increases the headloss by more than the resistance due to sand. This, combined with the increased usage of RO plants provides an opportunity for horizontal flow sand filters to be developed for water pretreatment.

Chapter 3-Methodology

3.1-Outline

This chapter will describe the methodology used in analysing the flow problem and determining an optimum configuration for the horizontal sand filter. The primary method of analysis will be using computational fluid dynamics (CFD) software. The CFD package being used is the FLUENT™ solver being used in conjunction with GAMBIT™ meshing software. Validation of the model will also be undertaken to confirm the results of the CFD software are accurate and to investigate other phenomena that cannot be modeled by the software.

3.2-Geometry

3.2.1-Outline

The basic geometry being analysed was identified by Mossad & Aral (2009); it consists of baffles placed in the upper part of the pipe. This geometry was chosen due to its simplicity which would make manufacturing in a commercial environment more viable. The key principle in this geometry is that the baffle obstructs the flow in the channeled area and forces the fluid downward, through the sand. This benefit is counteracted somewhat by the increase in pressure caused by the baffles blocking the flow.

3.2.2-Basic Geometry

The geometry to be modeled will have an inner diameter of 0.2 metres and a length of 10 metres. This basic geometry is shown below.

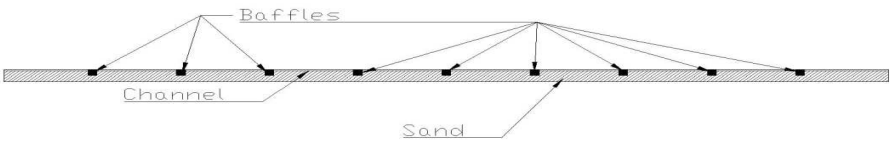

Figure 3.2.1 -Basic Geometry of the Horizontal Sand Filter

This is the original geometry to be anaylsed with the CFD software; further modifications to the size, shape, angle, thickness and spacing of the baffle is done based on the numerical solutions, fundamental fluid laws and Darcy's law. The objective of the optimization process is to reduce the velocity and hence flow rate of fluid through the channeled section of the pipe while minimising the pressure requirements of such a setup.

3.2.3-Dimensionless Analysis

Dimensionless analysis allows is useful in numerical modeling because it provides a solution that is useful in many situations. The principle behind dimensionless analysis is to define a functional relationship based on dimensionless parameters for any given system, this relationship should then be correct for all variations of the flow as long as the dimensionless values stay the same. The Buckingham Pi theorem was used to determine the dimensionless parameters relevant to this flow problem. The dimensionless Pi groups determined for this problem are given as:

$$\Delta p = f(\rho, V_s, D, \mu, \epsilon, k, g)$$

$$\Pi_1 = \frac{\Delta p}{\rho {V_s}^2}$$

$$\Pi_2 = \frac{\mu}{\rho V_s D}$$

$$\Pi_3 = \frac{k}{d^2}$$

$$\Pi_4 = \frac{Dg}{V_s^2}$$

$$\Pi_5 = \epsilon$$

$$\Pi_1 = f(\Pi_2, \Pi_3, \Pi_4, \Pi_5)$$

These non-dimensional groups fit the theories of du Plessis & Diedericks (1997) and Binnie et. al. (2002) who determined that the Reynolds number (Π_2) in between the pores is a function of the superficial Reynolds number and porosity.

3.3-Meshing and Modelling using GAMBIT™

GAMBIT™ is the default grid generation software used by FLUENT™, it has the capability to create and mesh geometries in 3 dimensions for export into FLUENT™. Other mesh generation and CFD software such as CFX was investigated for use however due to its compatibility with the FLUENT™ software GAMBIT™ was the preferred choice.

The horizontal filter was drawn in GAMBIT on a 1:1 scale from the original geometry. As the sand filter is symmetrical along the vertical axis a symmetry boundary condition could be imposed along the axis meaning that less computing power is needed to achieve the same results, allowing for quicker solution times or more accurate and dense meshes if it is required.

The meshing of the model is the most important step in the CFD model generation process, and it is important to determine the critical points in the geometry that need to be modeled accurately or that have high velocity/pressure gradients as the mesh should be finer in these regions. The diagram below is an outline of the points of importance in the geometry and locations where the mesh needs to be fine.

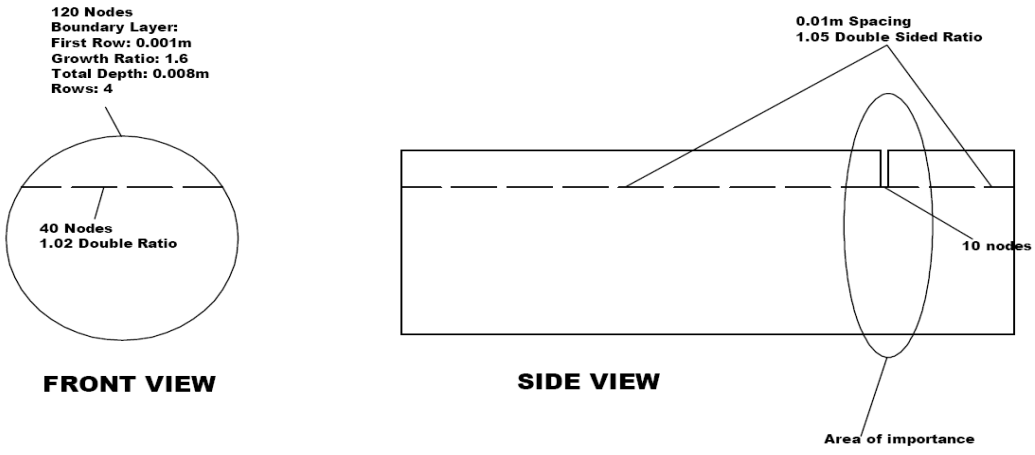

Figure 3.3.1 -GAMBIT Meshing overview

The number of cells varied with the geometry but ranged from 1 million to 2 million cells.

Detailed meshes for specific geometries are provided in appendix C.

3.4-FLUENT™ Solver

The FLUENT™ Solver is a computational fluid dynamics solver capable of solving many fluid flow problems for laminar, turbulent, multiphase and non-Newtonian flow problems. In addition it is capable of modeling chemical reactions and combustion as well as flow through porous media. The FLUENT™ solver was chosen because of its capabilities in modeling flow through porous media as well as the ability for problems to be customized using User Defined Functions (UDF's).

3.4.1-FLUENT™ solver setup

FLUENT™ has two numerical solvers to choose from, a pressure based solver and a density based solver. While both solvers have recently been modified to be able to model all types of flow, historically pressure based solvers have been used to model low-speed incompressible flow and thus will be used to solve this problem (FLUENT™ User Guide).

The flow problem is governed by the continuity and Navier-Stokes (momentum) equations which FLUENT™ solves. In this case the flow assumed to be steady, incompressible, laminar and Newtonian. In this situation the governing equations can then be simplified to:

$$\frac{\partial u}{\partial x}+\frac{\partial v}{\partial y}+\frac{\partial w}{\partial z}=0$$

$$\rho\left(u\frac{\partial u}{\partial x}+v\frac{\partial u}{\partial y}+w\frac{\partial u}{\partial z}\right)=\rho g_x-\frac{\partial p}{\partial x}+\mu\left(\frac{\partial^2 u}{\partial x^2}+\frac{\partial^2 u}{\partial y^2}+\frac{\partial^2 u}{\partial z^2}\right)+S_x$$

$$\rho\left(u\frac{\partial v}{\partial x}+v\frac{\partial v}{\partial y}+w\frac{\partial v}{\partial z}\right)=\rho g_y-\frac{\partial p}{\partial x}+\mu\left(\frac{\partial^2 v}{\partial x^2}+\frac{\partial^2 v}{\partial y^2}+\frac{\partial^2 v}{\partial z^2}\right)+S_y$$

$$\rho\left(u\frac{\partial w}{\partial x}+v\frac{\partial w}{\partial y}+w\frac{\partial w}{\partial z}\right)=\rho g_z-\frac{\partial p}{\partial x}+\mu\left(\frac{\partial^2 w}{\partial x^2}+\frac{\partial^2 w}{\partial y^2}+\frac{\partial^2 w}{\partial z^2}\right)+S_z$$ [4]

(FLUENT™ User Guide & Fox et. al 2009)

[4] S_x, S_y and S_z are source terms added to the momentum equations to account for the porous conditions.

The FLUENT™ solver also has a selection of methods to choose from in relation to the discretization of the pressure gradient. The FLUENT™ user guide recommends the use of the 'PRESTO!' scheme for porous media; this scheme uses a staggered control volume in order to determine the staggered pressure difference across a face. This process is similar to the process used to create staggered grids in structured meshes like the one identified by Katsaounis and Levy (1998).

The final option relevant to this flow problem is whether to use the superficial or physical velocity of the porous media. Experience with the model has shown that when using the superficial velocity formulation, the solution is incorrect since the pressure values are too low. Therefore the physical velocity formulation was used.

3.4.2-Boundary Conditions

Inlet Velocity

The inlet velocity is the initial velocity at the inlet of the horizontal sand filter. The velocities for the actual sand filter will vary between 0.0015 and 0.005 m/s depending on targeted flow rates. As a baseline to compare geometries, a velocity of 0.005 m/s will be used since it coincides with the average loading rates found in the literature review.

Gravity

Gravity is an important force in this problem since it is the force that is responsible for the settling of the sand, and at the larger diameter geometries gravity may help in forcing the flow downwards through the sand.

Operating Pressure & Outlet

The outflow in the horizontal sand filter model will be a simple pressure outlet at 0 gauge pressure. It is important to then set the operating pressure at atmospheric pressure (101.3kPa) at the centre of the pressure outlet. In most cases this will be at X=10, Y=0, Z=0.

Porous Medium

In flows through porous media, a source term S_i is included in the momentum equation as shown in section 3.4.1. Equation 7.19-1 in the FLUENT™ User Guide shows this equation as:

$$S_i = -(\sum_{j=1}^{3} D_{ij}\mu v_j + \sum_{j=1}^{3} C_{ij}\frac{1}{2}\rho|v|v_j)$$

Where S_i is the source term in the momentum equation in x, y or z. This force term contributes to the pressure gradient in the cell, creating a pressure drop proportional to velocity as described by Darcy's law. The second part of the equation relates to inertial loss, which can be ignored in laminar flow cases. Therefore, in the case of a homogenous porous medium (such as in this case) the source term simplifies to:

$$S_i = -(\frac{\mu}{\alpha}v_i)$$

Or

$$\nabla p = -\frac{\mu}{\alpha}\vec{v}$$

(FLUENT™ User Guide)

The above equation is the same relationship that Vafai (2000) described and was discussed in the literature review. From this relationship we note that for this flow situation the FLUENT™ solver requires the viscous resistance term, which is the inverse of the permeability (FLUENT™ User Guide) and the porosity of the medium.

As shown in chapter two, the accuracy of the calculated values of permeability are in doubt, therefore until experiments are done to validate the permeability of actual filter sand the permeability and porosity values from Ward (1964) will be used. The sand Ward used has a similar diameter and porosity to that of standard filtration sand and therefore could be deemed as suitable. The viscous resistance coefficient is therefore around 28.57×10^8 m^{-2} and the porosity is 0.4.

The sand was shown experimentally to settle to 95% of its original volume (Mossad & Aral 2009). In order to represent this in the numerical model, the porous medium was customized through the use of a User Defined Function. This function alters the viscous resistance term between the settled area and the channel and is written in a form of the C+ programming language. The viscous resistance of the channeled area was assumed to be around three orders of magnitude less than the resistance of the sand (i.e. from 10^9 to 10^6). An example of the UDF is given in appendix B. A spreadsheet of the calculated channel height in relation to the channels cross sectional area is provided in appendix D.

3.5-Experimental Validation

3.5.1-Overview

In order to estimate the level of uncertainty in the numerical model, the results need to be compared to experimental values. The model will be validated using the guidelines of AIAA-G-077-1998. In this case, the complete system will be tested; mainly because combining results from subsystem, benchmark and unit cases are outside the scope of this project. As the guide states, complete systems should contain 'all the essential flow physics' in order to be accurate and should be tested mainly to determine the accuracy of the grid rather than the accuracy of the numerical formulas or the interaction between different phenomena.

In order to get validation with an acceptable level of uncertainty, all boundary conditions need to be accurately determined and measureable. As explained before, there are issues with determining the permeability of the sand and therefore testing needs to be carried out on the filtration sand being used for validation to get an accurate permeability result. Once this has been determined, testing can then be done on the complete system case.

There are additional benefits to using a complete system case, one of which is that the effects of other phenomena that cannot be modeled accurately and easily, such as permeability and porosity changes with pressure can be determined. A dye could also be used to calculate the residence time and get a visualisation of how the flow progresses through the medium for extra validation. Therefore, in order to get suitable levels of uncertainty two experiments need to be carried out:

1. *Permeability Calculation:* This experiment is relatively straightforward and measures the permeability of the filtration media using a setup similar to the one Darcy used. This will validate the permeability figures as there are numerous formulas for the calculation of permeability and each one gives a different value of permeability. The method for calculating permeability will be taken from the FLUENT™ User Guide (Page 7-124)

2. *Complete System Validation:* This experiment is done according to AIAA-G-077-1998 and will measure the head loss across the sand filter and across a baffle along with measuring exit velocity profiles in order to validate the results given by the CFD software. The flow rate and initial pressure needs to be fixed in order to get accurate results. Additionally the filter will be inspected visually with dye to see if there is any channeling of the sand around the baffles.

3.5.2-Permeability Calculation Experiment

This experiment is very simple and will measure permeability using the principle of Darcy's law ($Q = \frac{-kA}{\mu}\frac{\Delta P}{L}$). Several tests are undertaken to ensure that an accurate permeability value is calculated and that the flow is completely saturated.

Figure 3.5.1 -Permeability experiment basic overview

In the above setup, the water is kept at a constant head and the flow rate is determined by measuring the volume of water collected and dividing it by the time taken to collect the sample.

From these measurements, all the inputs for the FLUENT™ User Guide's method of calculating permeability are available.

The general form is:

$$\frac{{}^{\Delta p}/_{v}}{\mu \Delta n} = \frac{1}{\alpha}$$

Where:

$$\Delta p = \rho g h_2$$

$$v = \frac{Q}{A}$$

$$\Delta n = h_1$$

Equipment

The important equipment utilised in this experiment was:

- PVC Pipe: 0.1 m Diameter by 1m length
- Filtration Sand: 0.55-0.65 mm effective diameter
- Screen to hold sand in place
- Graduated Cylinder: 2L, ±10mL accuracy at 20°C

Process

1. Measure the height of the sand from the bottom of the PVC column
2. Slowly pour water down the filter from the top, until water starts coming out the bottom
3. Get a decent head of water above the sand (4cm)
4. Connect up the constant head apparatus
5. Place an empty bucket underneath the filter and start the stopwatch
6. When a suitable amount of water has been collected, record the time on the stopwatch and remove the bucket from underneath the filter.

7. Measure the volume of water collected and record it
8. Repeat the experiment for better accuracy

Error Discussion

There are a number of possible errors that could occur during this experiment which would affect the permeability result. Firstly, if the sand column is not completely straight the calculated velocity could be out by a margin of $v\cos\theta$, which gives a maximum error percentage of 3.4% if within 15 degrees of vertical for a 1m long pipe.

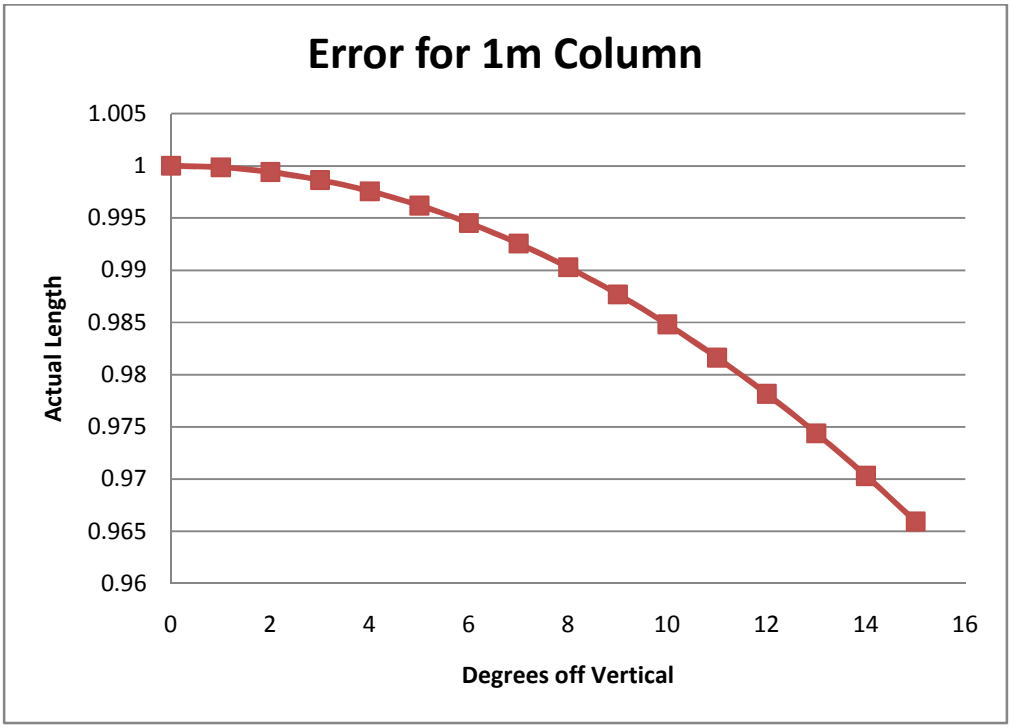

Figure 3.5.2-Plot of errors for non-vertical column

Another possible source of error in the estimation of permeability is the assumption of homogeneity, while the filtration sand has been graded and washed according to AWWA B100-89[5] there is still a degree of variability in the permeability, especially when considering the permeability changes with depth due to the weight of the water. Using a long length of pipe, in

[5] Further investigation of the sand properties is beyond the scope of this project. For more information go to http://www.riversands.com.au/divisions_waterfiltration.php

this case close to 1m helps reduce the effect of these errors but there still will be some degree of uncertainty.

The final source of experimental error is in the screen that holds the sand in place, figure 3.5.2.2 below shows the device used.

Figure 3.5.3-Screen

The screen consists of a stormwater grate covered with a bandage which stops the sand but is still porous enough to let water travel through freely. Tests have shown that the pressure difference through the screen is negligible and should not affect permeability results significantly.

The last source of error is measurement error brought about by the 5% inaccuracy of the measuring cylinder at room temperature. This is the largest calculable error in this test and represents quite a significant difference. There are several strategies that can be employed to reduce the significance of this error however, such as using large volumes so that the overall volume of error is negligible compared to the total volume and averaging several test results to cancel potential errors out.

3.5.3-Complete System Validation

This experiment is designed to validate the CFD results by evaluating the pressure difference between the sand filter and across a baffle in addition to comparing velocity profiles at the exit of the filter. A dye will also be used to visualise the flow better and measure residence times. All tests will be done at constant flow rate and pressure head to get accurate results. The detailed experiment setup is shown in Appendix E. It consists of a Perspex tube with five 2mm Perspex baffles spaced within the filter media since this captures all the essential flow physics in order to ensure our model is validated in accordance with AIAA-G-077-1998.

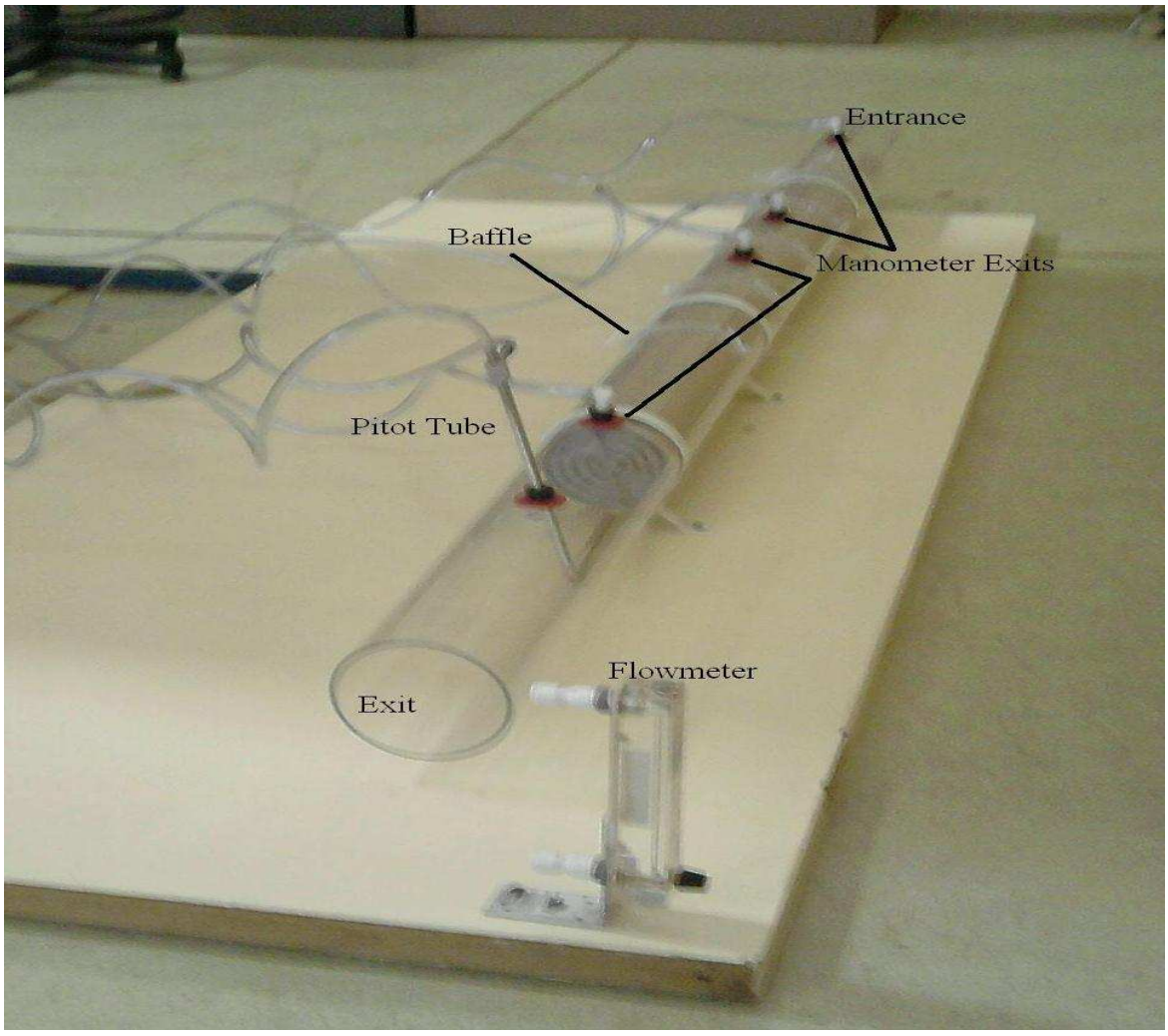

Figure 3.5.4-Complete System Setup

Equipment

The important equipment utilised in this experiment is:

- Constant head apparatus
- Flowmeter: Dwyer Instruments VFB-82 BV
- Pitot tube: Dwyer Instruments 160-8
- U Tube Manometer: Dwyer Instruments 1221-100
- Filtration Sand: 0.55-0.65 mm effective diameter
- Screen to hold sand in place
- Perspex tube: 104mm ID, 110mm OD x 2 metres
- 2mm perspex sheet for baffles
- Additional manometer tubes to determine pressure difference

Process

1. Setup the equipment in accordance with Appendix E.
2. With the filter in a vertical position and exit flowmeter closed, slowly fill it with water until the entire tube is full of water and no air gaps are present.
3. Close the Inlet tap and lay the filter horizontally, lightly tap the tube to ensure an evenly distributed sand layer.
4. Connect up the constant head arrangement and open the tap
5. Slowly open the flow meter tap until the desired flow rate is achieved
6. Record all manometer measurements at the desired flow rate
7. Record velocity profiles using the pitot tube
8. Investigate the filter for any other channeling or unintended flow phenomena.
9. Change the flow rate and repeat steps 2 thru 5

Additionally, when the dye is used the time taken for the dye to reach the end of the filter medium will be timed and filmed for better investigation.

Error Analysis

In order for the numerical model to be validated the data uncertainty needs to be estimated as suggested by Stern et. al (2001). In this case there are two types of uncertainty:

- *Quantifiable uncertainty*-This is the uncertainty that can be determined through data sheets or calculated and should give a percentage of accuracy of the result.
- *Unquantifiable uncertainty*-These errors cannot be quantified accurately and usually are the result of assumptions used in the experiment.

Quantifiable Uncertainty

Quantifiable uncertainty comes from the equipment used such as the flowmeter, Pitot tube, manometers, and filtration sand:

Flowmeter

From the Dwyer Instruments data sheet on the VFB series flowmeter (Appendix F), the accuracy of the flowmeter is 3% of the full scale. In this case the full scale is 30 cc/min, giving a maximum error of ±0.9 cc/min. Considering that the flow rates measured are going to be in the lower region of between 2-5 cc/min this error is quite significant. Since the flowmeter is being used to regulate the overall velocity within the pipe, this error magnifies the error of the pitot tube measurement. Errors from this measurement however can be reduced during validation by modifying the numerical model to having a pressure inlet instead of a velocity inlet. The absolute velocity error due to the flowmeter can be expressed as:

$$|V_{FE}| = \frac{1.5 \times 10^{-4}\, m^3/_S}{A}$$

Which is important in determining the total error of the pitot tube.

Pitot tube

The Dwyer Instruments 160-8 pitot tube has a calibration factor of 1, meaning that a straight reading can be taken from the pressure difference to convert it to a velocity value. Fox et. al (2009) describe the formula for calculating velocity from the pressure difference as:

$$V = \sqrt{\frac{2\Delta p}{\rho}}$$

The Dwyer Instruments data sheet (Appendix F) states that the accuracy of the pitot tube is 2% provided it is within 5 degrees of the actual velocity, because of a relationship similar to that identified in figure 3.5.2.2. In addition to this error, there is the error present in the flowmeter which affects the base velocity. Therefore for the velocity profile to be considered validated:

$$|V_{FE}| + |V_D \times 0.02| \geq V_S - V_D$$

Or in the case that the above equation is not satisfied, the validation uncertainty percentage is:

$$U = 1 - \frac{V_S - V_D}{|V_{FE}| + |V_D \times 0.02|} \times 100$$

Note that these relationships ignore the effect that any error in the pressure reading or permeability of the sand has on the velocity.

Manometers

The manometers measure the pressure difference using the relationship:

$$\Delta p = \rho g(h_1 - h_2)$$

The main source of error in this equipment is from the determination of the height difference, due to the inaccuracy of the tape measures. Assuming the inaccuracy of the tape measures are ±1mm (Level 1 standard) the maximum pressure error is:

$$\Delta p_E = \rho g(2mm)$$

At standard conditions:

$$\Delta p_E = 999 \times 9.81 \times 0.002$$

$$\Delta p_E = 19.6\ Pa$$

This error value is very small compared to the typical pressure requirements which are in the order of 10^4 Pa.

Unquantifiable Uncertainty

The unquantifiable uncertainty in the validation model comes from errors due to the assumptions, simplifications and oversights of the experimental model and numerical model (Chung, 2003). The main assumptions of the numerical model are that the flow is steady, laminar and incompressible; additionally it is assumed that the permeability and porosity of the sand is constant throughout the column. These assumptions are carried into the experimental model, with the assumption that the water's velocity profile is fully developed before it enters the sand layer.

Errors due to simplification arise from the deliberate simplifications imposed on the model in order to achieve a result. There has not been much simplification of this model in comparison to the numerical model. One major simplification of the numerical and experimental model is that pure water was used, instead of unfiltered water. The effect of the water quality was assumed to not have a significant effect on the flow within the filter and thus can be ignored.

Oversights are the errors due to accidental omission of one or several of the important parameters in the model. They are impossible to identify before the validation process and present a significant risk in the experiment. The only way to effectively minimise the chance of oversight error is to do extensive research into the flow phenomena.

Stern et. al (2001) discuss how there is no way to determine these errors, however introduce a simple method of determining the significance of them. In short

$$IF$$

$$|S - D| \gg E_Q$$

$$THEN$$

$$|S - D| \approx E_{UQ}$$

Considering that most of the assumptions and simplifications in this model are valid and will have minimal effects on the models, the uncertainty error will be due to a significant oversight error in this case and should be easily identified and included into the model.

Chapter 4-Numerical Results and Discussion

4.1-Original Geometries

The original geometry to be modeled comes from the work of Mossad and Aral (2009) and consists of baffles at 1 metre intervals that protrude to half the diameter of the pipe. This model and two variations of it were originally modeled with a rough mesh to determine what the flow looked like and which variation would lead to the least channeling and thus required a better investigation. The detailed numerical models are provided in appendix G.

Geometry 1 (Filename: 111-205-2707)

The baffles in this geometry are 20mm wide, 100mm deep and spaced 1 metre apart. The pipe is 200mm in diameter and 10 metres long. The mesh consisted of approximately 1.08 million nodes and was finer within the area of the baffles. Figure 4.1.1 shows the pressure contours around a baffle in this geometry.

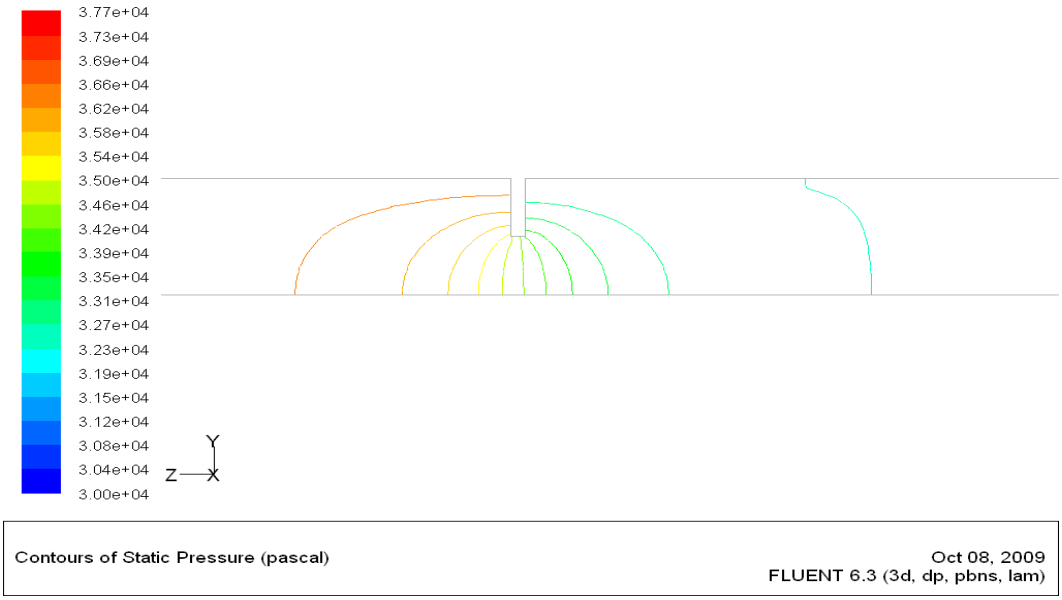

Figure 4.1.1-Pressure contours around a baffle

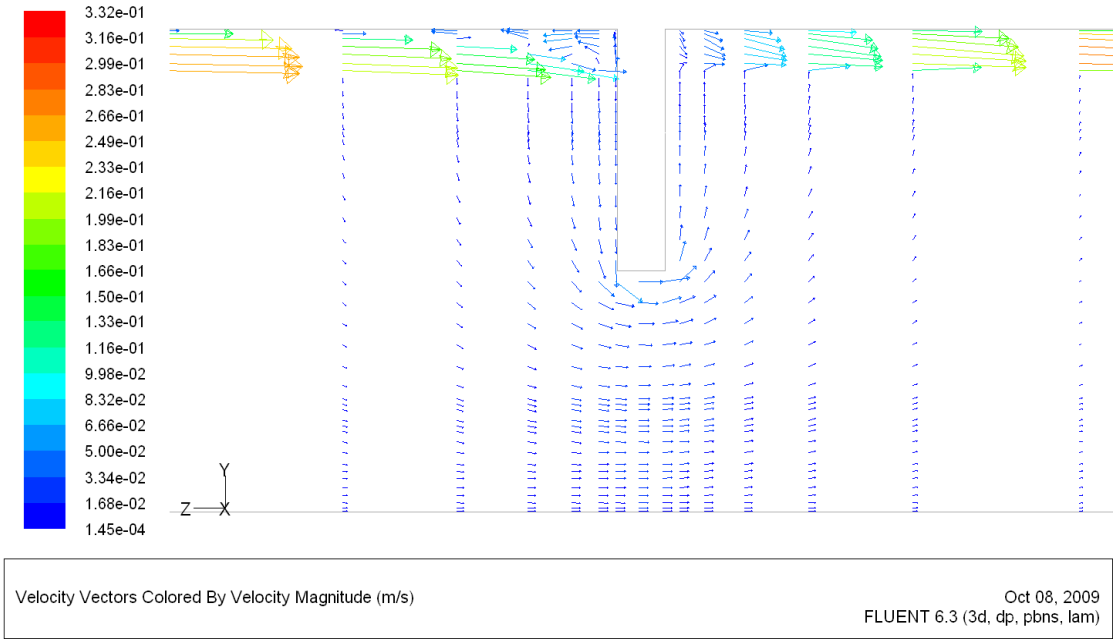

Figure 4.1.2-Velocity vectors around a 100mm baffle

The overall pressure difference in this case was 37.7kPa and the pressure drop across a baffle was 4kPa (taken 0.5 metres in front and 0.5 metres behind the baffle). In the Figure 4.1.2, the velocity vectors around a baffle are shown and show how significant the effect of channeling is. While the fluid flows underneath the baffle and increases velocity due to the conservation of mass, almost immediately after the baffle has ended the water finds its way to the channeled area.

Geometry 2 (Filename: 555-205-2307)

This geometry is exactly the same as that of the first geometry with the exception that the baffle is only 50 mm deep. The mesh consisted of 353 000 nodes and was equally spaced throughout the geometry; while this mesh is not as accurate it still provides good enough results to base further work with more refined meshes on. Figure 4.1.3 shows pressure contours around one of the baffles.

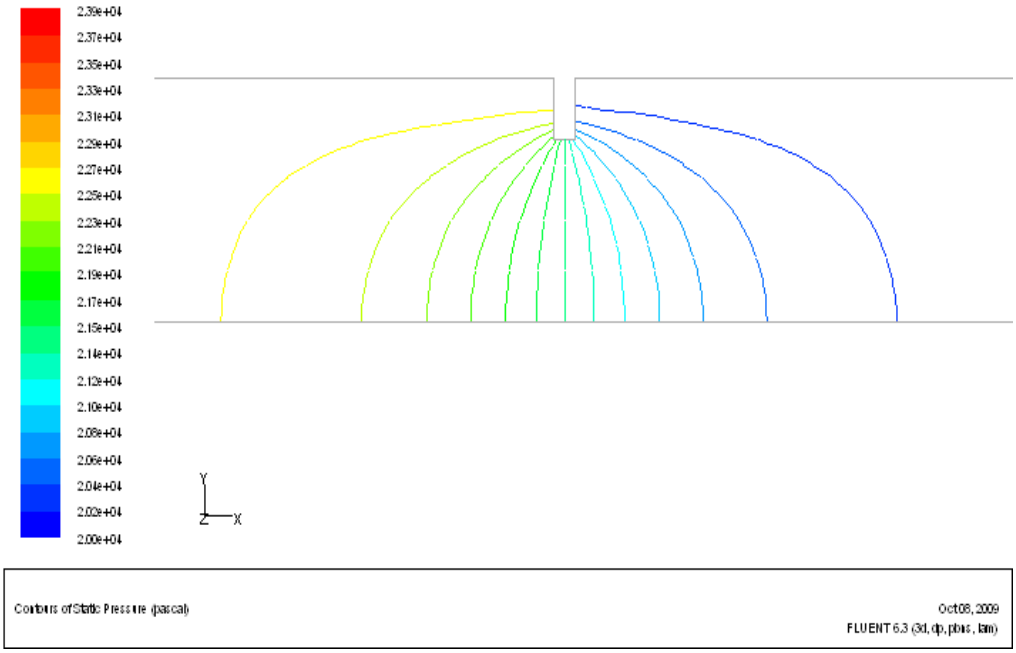

Figure 4.1.3-Contours of pressure around a 50mm baffle

The total pressure difference in this case was 23.9kPa and the pressure drop across a baffle was 2.5kPa (taken 0.5 metres in front and 0.5 metres behind the baffle). In the vector plot below it can be seen that the flow follows a similar pattern to the previous geometry. Of interest in this geometry is the pressure difference, which is not half that of geometry 1 as it was expected to be.

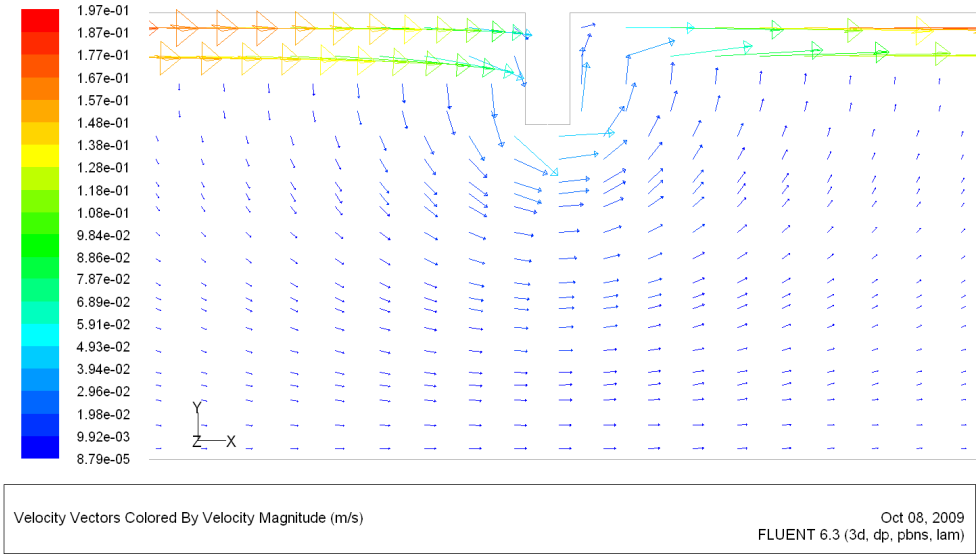

Figure 4.1.4-Velocity vectors across a 50mm baffle

Geometry 3 (Filename: 551-205-2707)

This geometry has the same depth as geometry 2, but is angled at 22° in the direction of the fluid flow. The mesh consists of 1.2 million nodes which is refined in the area close to the baffles. Figure 4.1.5 shows pressure contours around one of the angled baffles.

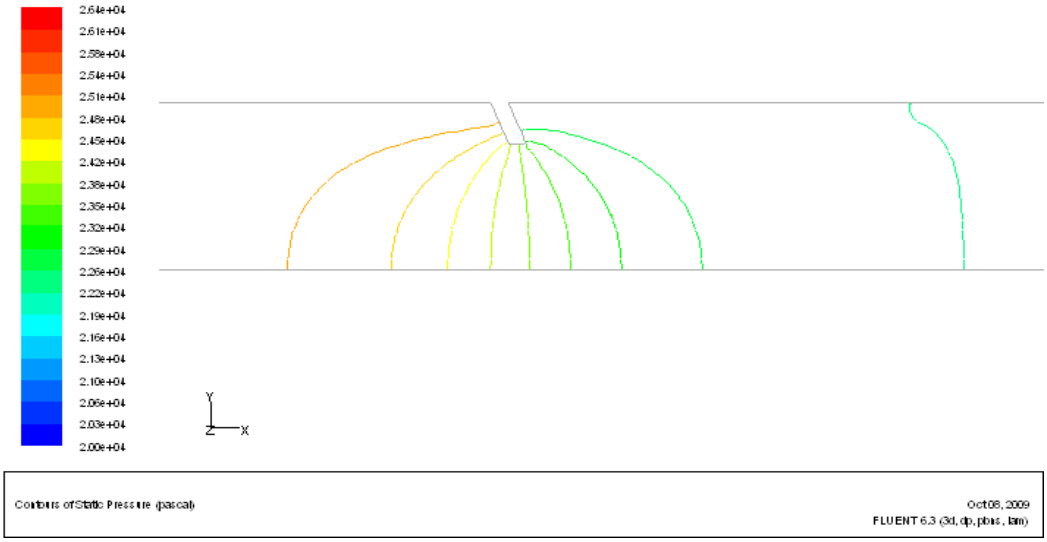

Figure 4.1.5 -Contours of pressure around a 22° baffle

The total pressure difference in this case was 24.1kPa and the pressure drop across a baffle is 2.5 kPa (taken 0.5 metres in front and 0.5 metres behind the baffle). This indicates that there is either a comparison error due to the unrefined grid of the previous geometry or that more fluid is flowing through the sand due to the creation of a large recirculation zone forcing more water to travel through the porous media. Figures 4.1.6 & 4.1.7 show that there is a recirculation zone both ahead and behind the baffle which will increase the amount of time the fluid stays in the sand. However it is debatable whether the angled baffle provides a clear benefit over a simple straight baffle and this needs to be examined further.

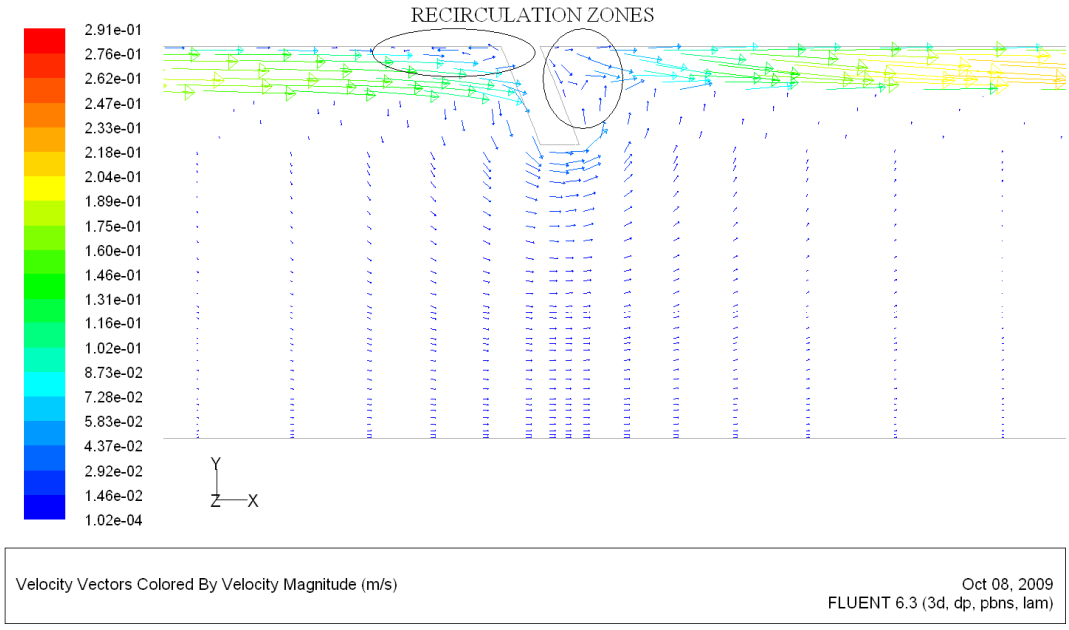

Figure 4.1.6-Vector plot across a 22° baffle showing recirculation zones

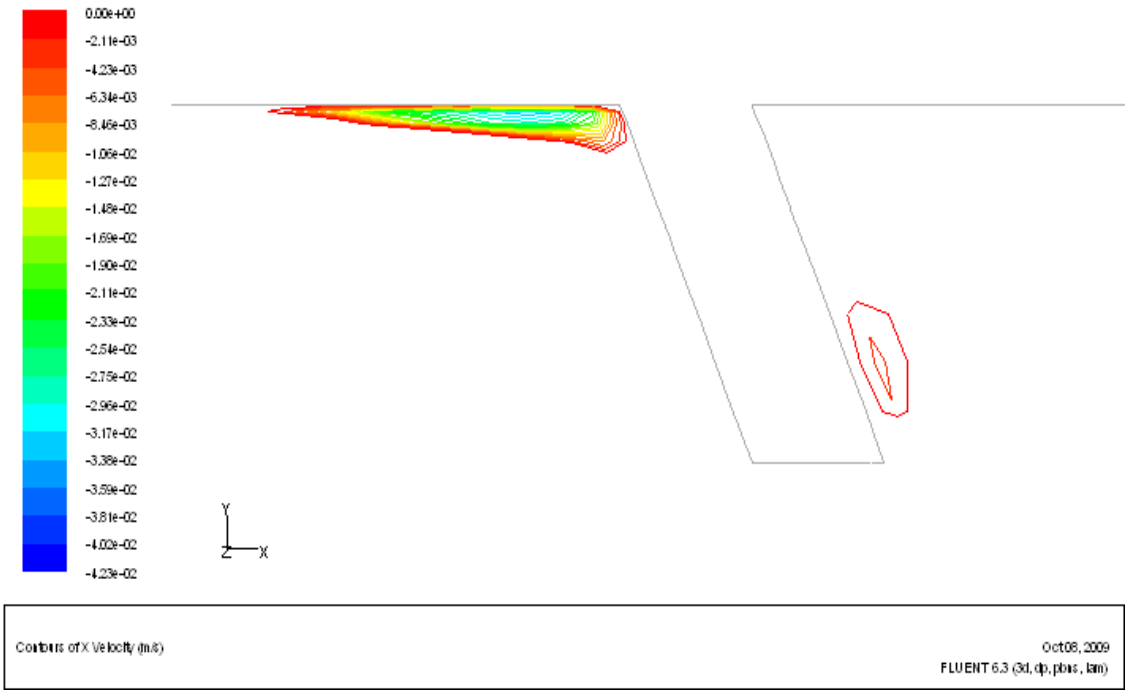

Figure 4.1.7-Contours of negative X Velocity, indicating recirculation zone location

Geometry 2a (Filename: 555-205-2707)

This geometry is similar to that of geometry 2, with the exception that the baffle is 2mm wide instead of 20mm and the spacing between baffles is 0.5 metres instead of 1 meter. The mesh has also been refined significantly to provide a better comparison with the angled baffle to determine which geometry should be investigated further as the optimum geometry. The mesh consists of 1.4 million nodes with good refinement at key points.

The pressure difference for this geometry is 41.6kPa, and the pressure difference across a baffle is 2.1kPa (0.25m ahead and behind the baffle). For comparison, the pressure difference at the same points in geometry 3 is 2.3kPa. Figure 4.1.8 shows the pressure contours across a baffle for this geometry.

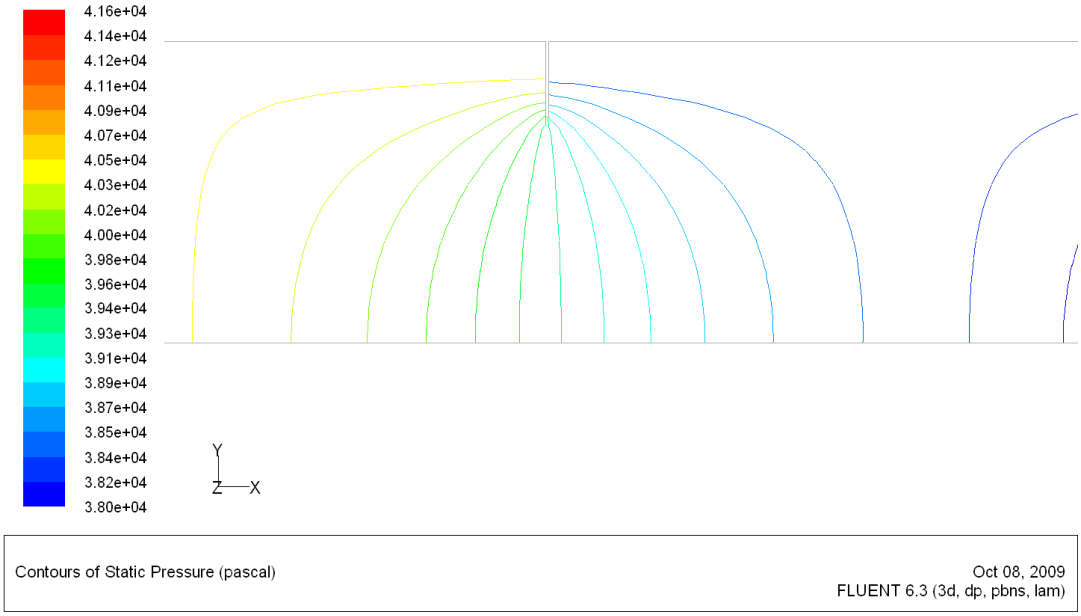

Figure 4.1.8-Pressure contours across geometry 2a baffles

Figure 4.1.9 is the vector plot for this geometry and it shows that recirculation zones exist to the same degree in this geometry as in geometry 3. Additionally, the recirculation zone ahead of the baffle is larger than geometry 3 at the expense of no recirculation zone behind the baffle.

It was decided that geometry 2a showed the most promise for further geometry optimisation because of the large recirculation zones that reduce the flow in the channelled area.

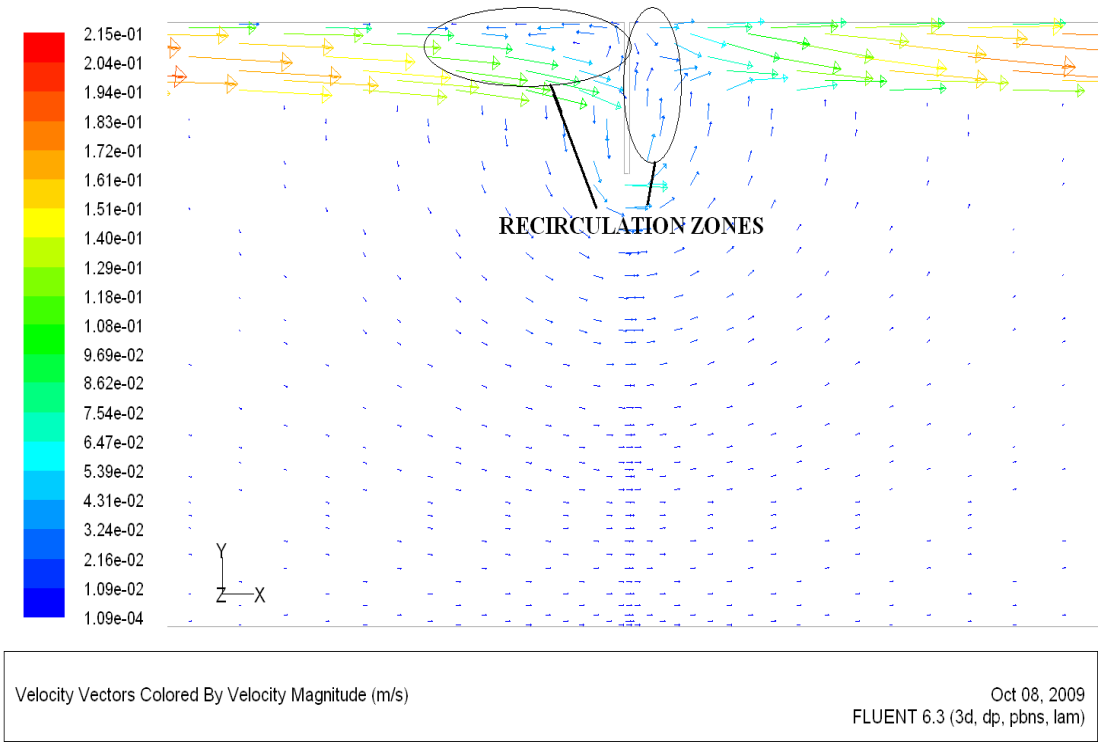

Figure 4.1.9-Vector plot across geometry 2a showing recirculation zones

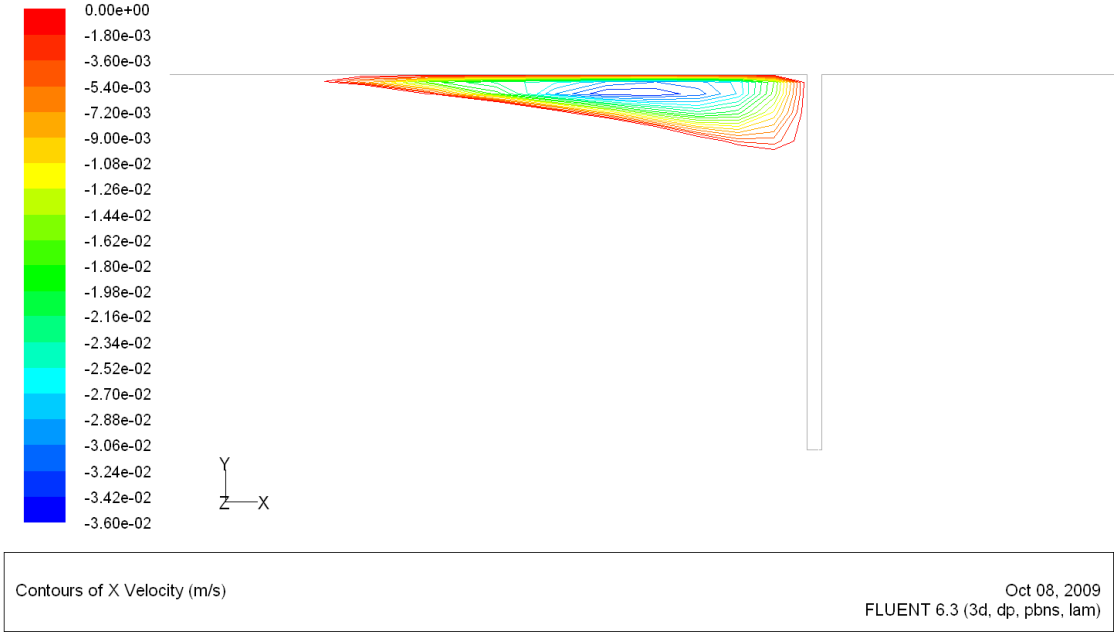

Figure 4.1.10-Contours of negative x velocity in geometry 2a

4.2-Geometry Refinement

Figure 4.2.1 is a plot of the velocity profile for geometry 2a before the fluid encounters the baffle [in green] compared to a fully developed profile [in blue], the negative velocity means that there is a recirculation zone before the baffle.

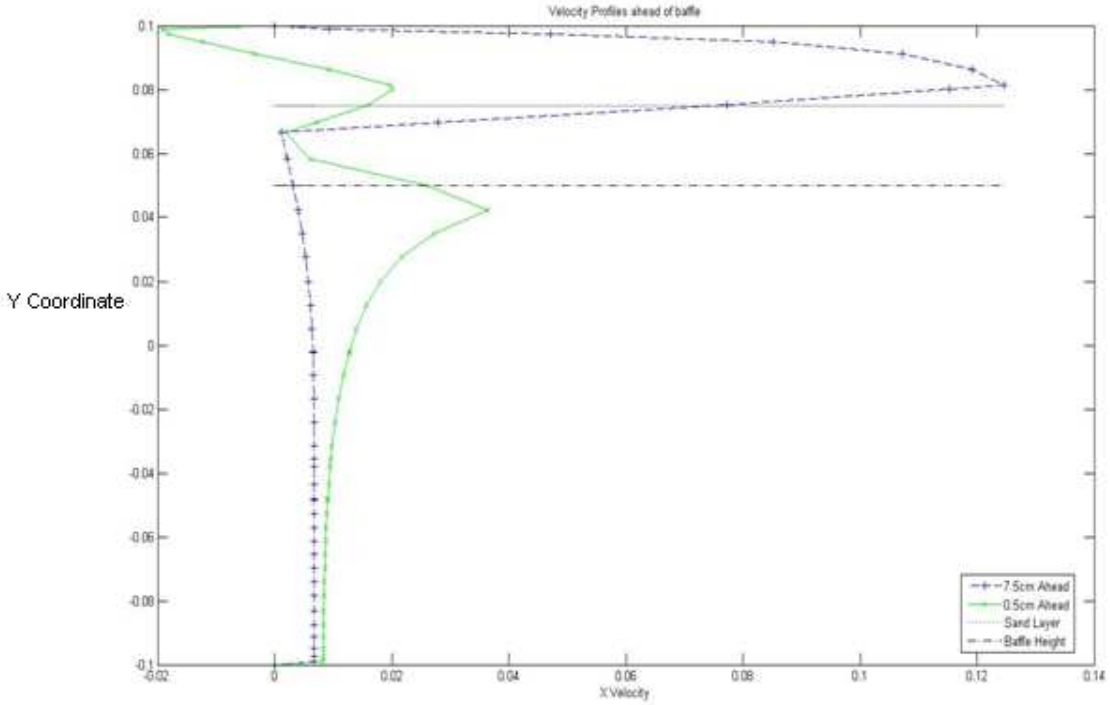

Figure 4.2.1-Velocity Profiles of geometry 2a before the baffle

The importance of this plot is to show the effect a baffle has on the velocity profile in both the channelled area and the porous media. As can be seen, the velocity profile in the channelled area is fully developed 7.5 cm before it reaches the baffle and shows a fairly typical laminar type profile whereas the velocity profile just before the fluid hits the baffle is disrupted significantly.

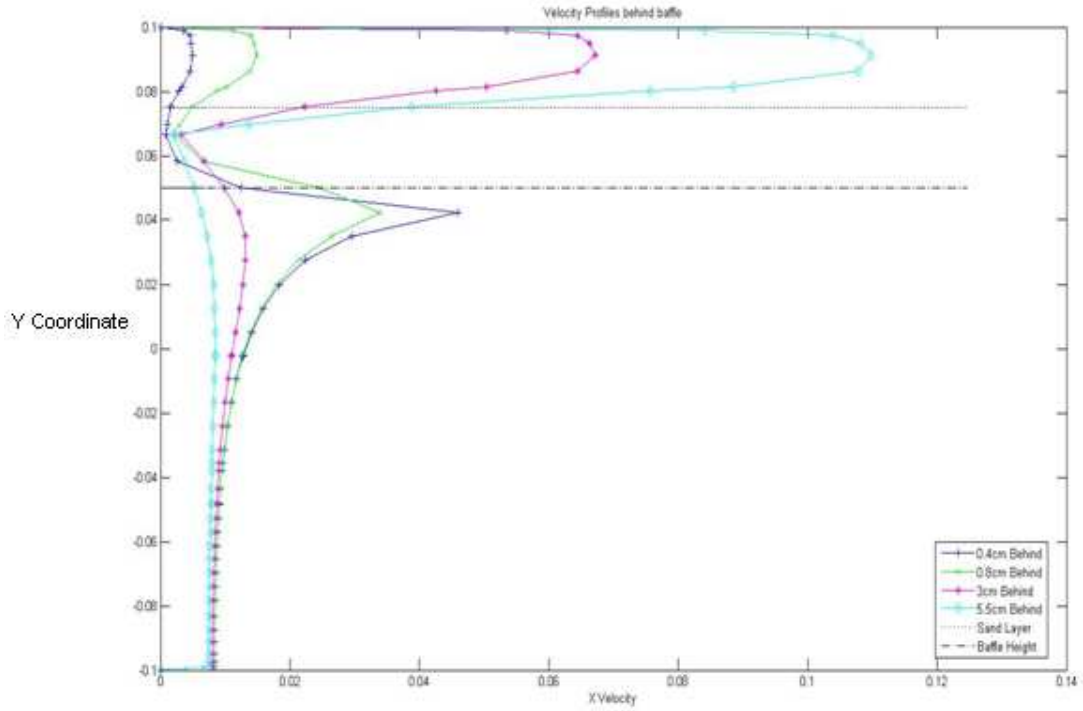

Figure 4.2.2-Velocity Profiles after Baffle

Figure 4.2.2 is of the velocity profile after the baffle. From this plot it can be seen that after about 5cm the velocity profile in the sand area (under 7.5 x 10^{-2}m) is still affected by the baffle but within the channeled area, the profile is fully developed.

From these two diagrams it can be seen that the velocity profile of the fluid is significantly disrupted in the region around the baffle and the fluid travels through the sand at a higher velocity for some distance before and after the baffles. Additionally any modifications to the geometry needs to occur in the area around the baffle where the velocity profile is not fully developed to reduce the pressure requirements.

Geometry 4 (Filename: 556-2005-2907)

The first modification made to geometry 2a was to add a second baffle of the same height 4mm behind the first baffle. This no longer makes the channeled area the path of least resistance and therefore forces the fluid to flow beneath the baffles. In order to get a better mesh, the geometry was shortened to 2.5m. The grid has 1.2 million nodes and is refined around the double baffles.

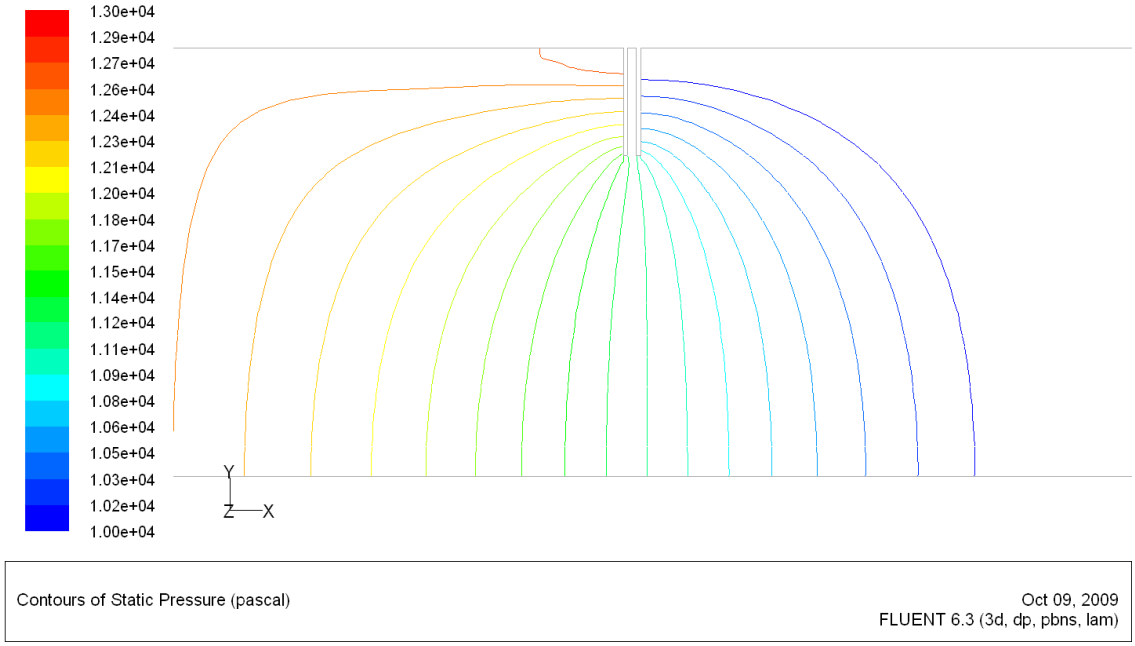

Figure 4.2.3-Pressure Contours across a baffle in Geometry 4

The total pressure drop in this case is 10.11kPa, by comparison a 2.5 meter section with a single baffle has a total pressure drop of 9.69kPA. Across both baffles, the pressure drop is 2.2kPa which compares favourably with a pressure drop in the single baffle geometry of 2.1kPA (taken 0.25m ahead and behind the baffle).

Figure 4.2.4 shows the velocity vectors around the double baffle, it shows that the fluid completely bypasses the area between the baffles and instead continues through the sand.

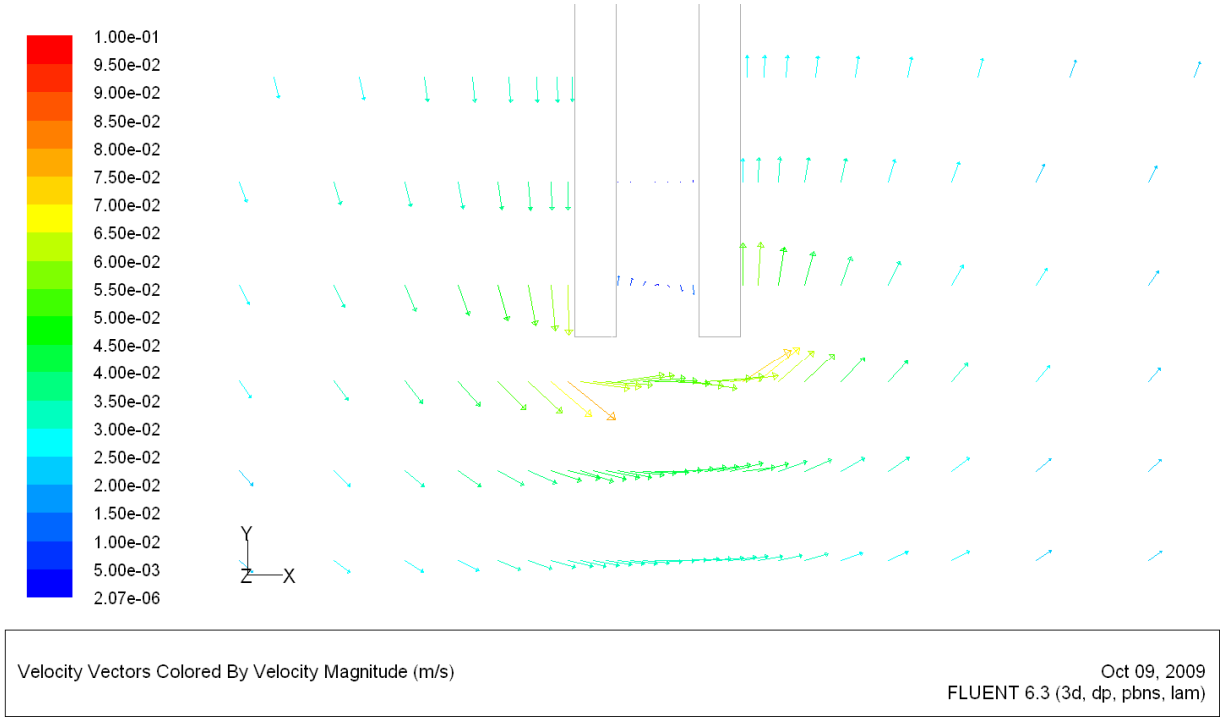

Figure 4.2.4-Velocity Vectors across a baffle in geometry 4

A plot of the velocity profiles in geometry 4 (Figure 4.2.5) reinforces this observation, showing that there is no flow between the baffles.

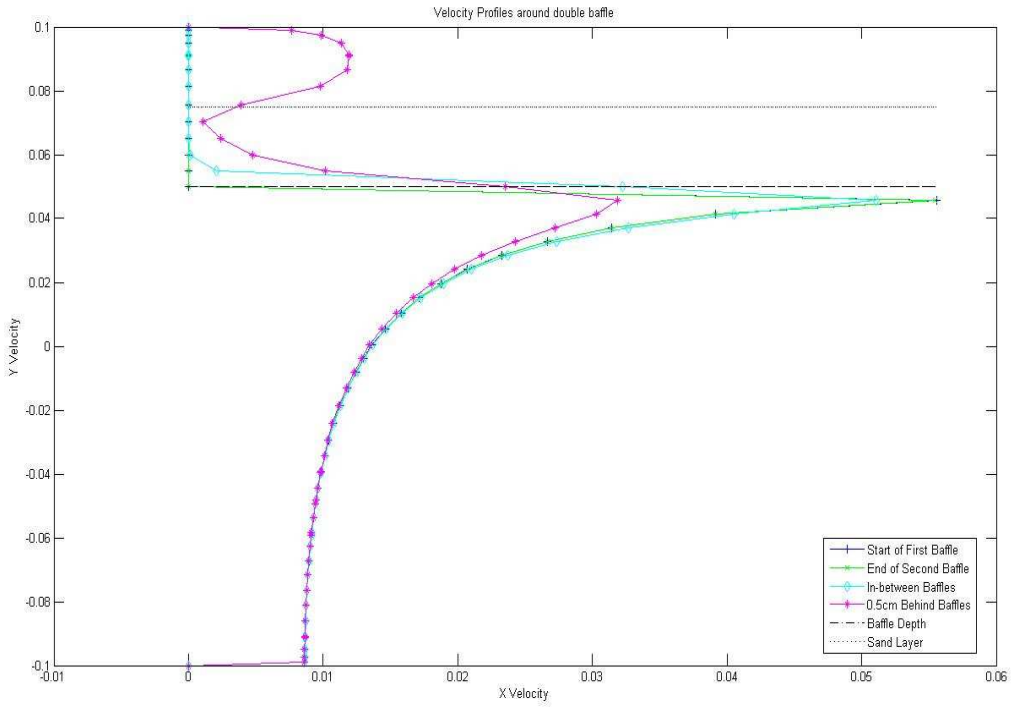

Figure 4.2.5-Velocity Profiles in Geometry 4

The benefit of this geometry is quite obvious, completely eliminating the fluid flow in the channelled area for a minimal increase in pressure, which is to be expected due to the increased amount of fluid within the porous medium.

Geometry 5 (Filename: 754-2005-0308)

This geometry is a modification of geometry 4. In this case the second baffle is 2.5cm deeper than the first baffle and is still 4mm behind it. It was hoped that the pressure effect of adding a deeper baffle would be reduced if a shorter one was placed in front of it. The benefit to a deeper baffle would mean that baffles could possibly be spaced further apart which makes the fluid stay in the porous medium for longer.

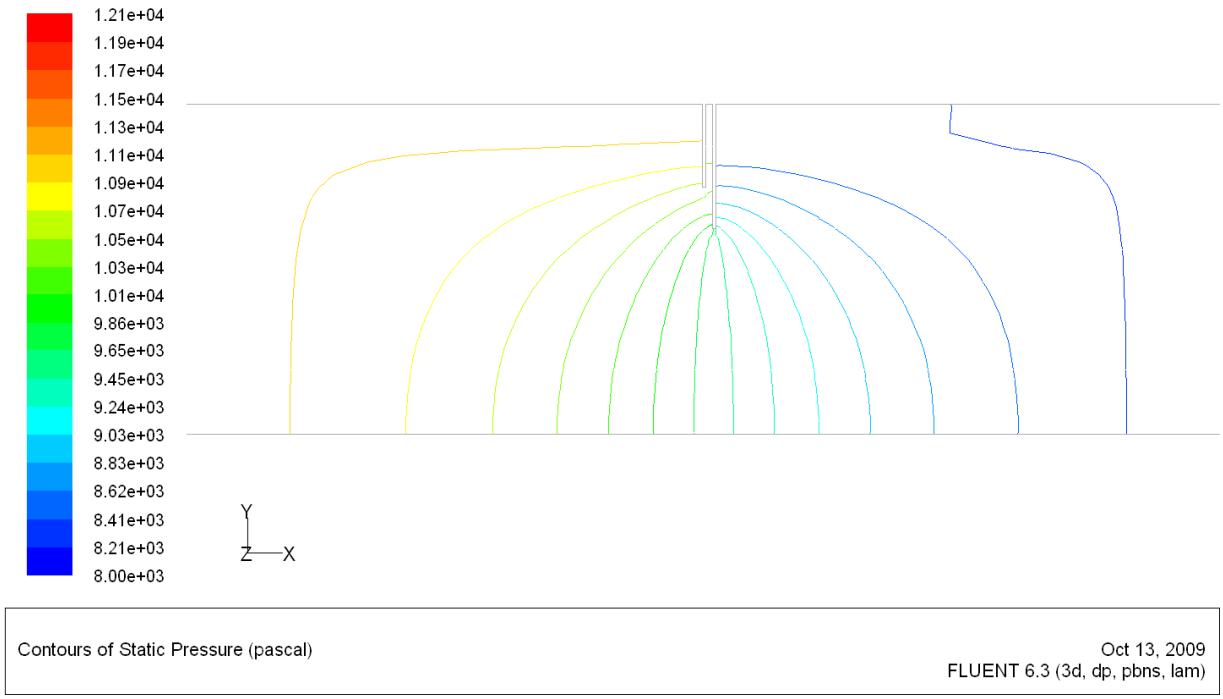

Figure 4.2.6-Pressure Contours across a baffle in geometry 5

The total pressure drop in this geometry is 12.13kPa, and across one set of baffles is 2.7kPa. These pressure difference terms indicate that the geometry is not doing what was hoped and reducing the effect of a deeper baffle on the pressure difference. However the benefit of a deeper baffle is that it takes longer for the fluid to travel back up to the channelled area and therefore the velocity profiles should be different. As figure 4.2.7 shows, the velocity profiles are different, having higher velocities in the sand layer due to the conservation of mass principle. An important observation of this diagram is the velocity of the fluid in the channelled area 0.5cm after the baffle, it is lower than that in geometry 4 (figure 4.2.5) however not by a significant amount.

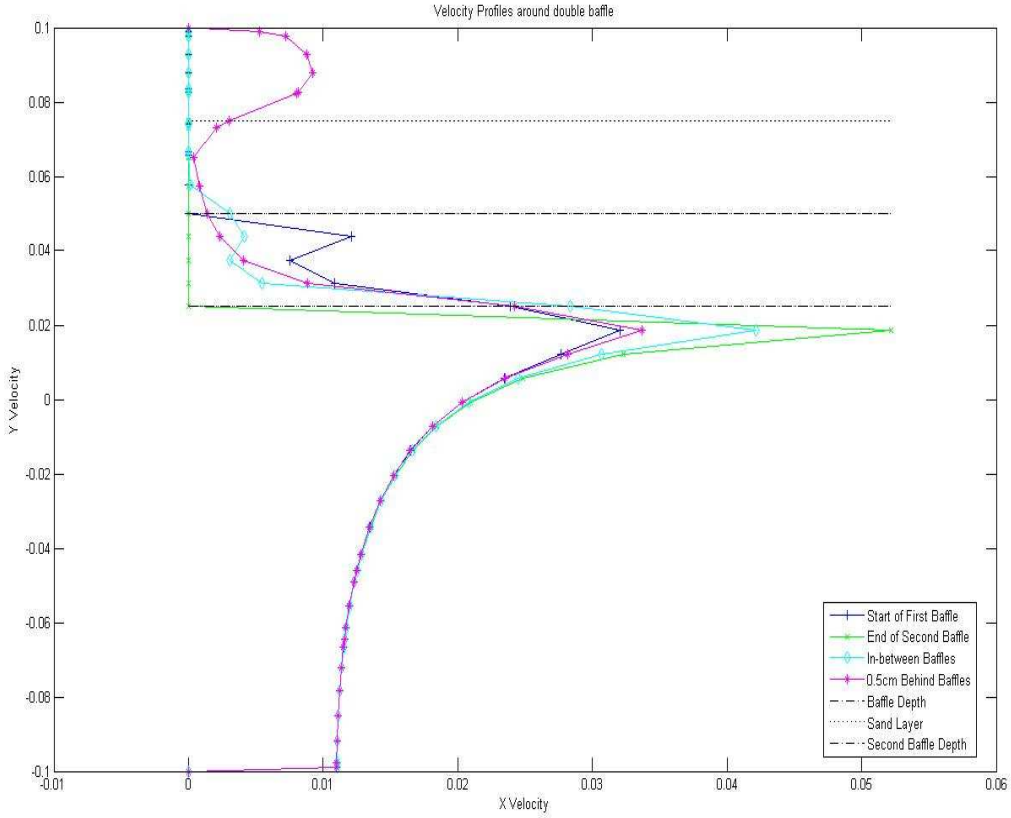

Figure 4.2.7-Velocity profiles around baffles in geometry 5

Considering the increased pressure requirements for a minimal change in the flow throughout the profile, it is concluded that this geometry is not optimal. Therefore geometry 4 is considered the ideal configuration, and more investigations need to be done on determining the optimal spacing of the baffles.

4.3-Geometry Optimisation

The optimum geometry, as discussed above is geometry 4 which consists of baffles that are ¼ of the diameter of the pipe spaced close together. In order to determine the optimal spacing, the pressure difference between the baffles and the velocity of water through the channelled area will be compared for different baffle spacing's.

To save on computing time, the grid of geometry 4 was used and scaled in the x direction to get the desired distance between the end of the first and start of the second baffle. Since the diameter and therefore the area of the pipe stays the same, the pressure differences will still be comparable provided they are taken at the same position in line with the inner edges of the baffle.

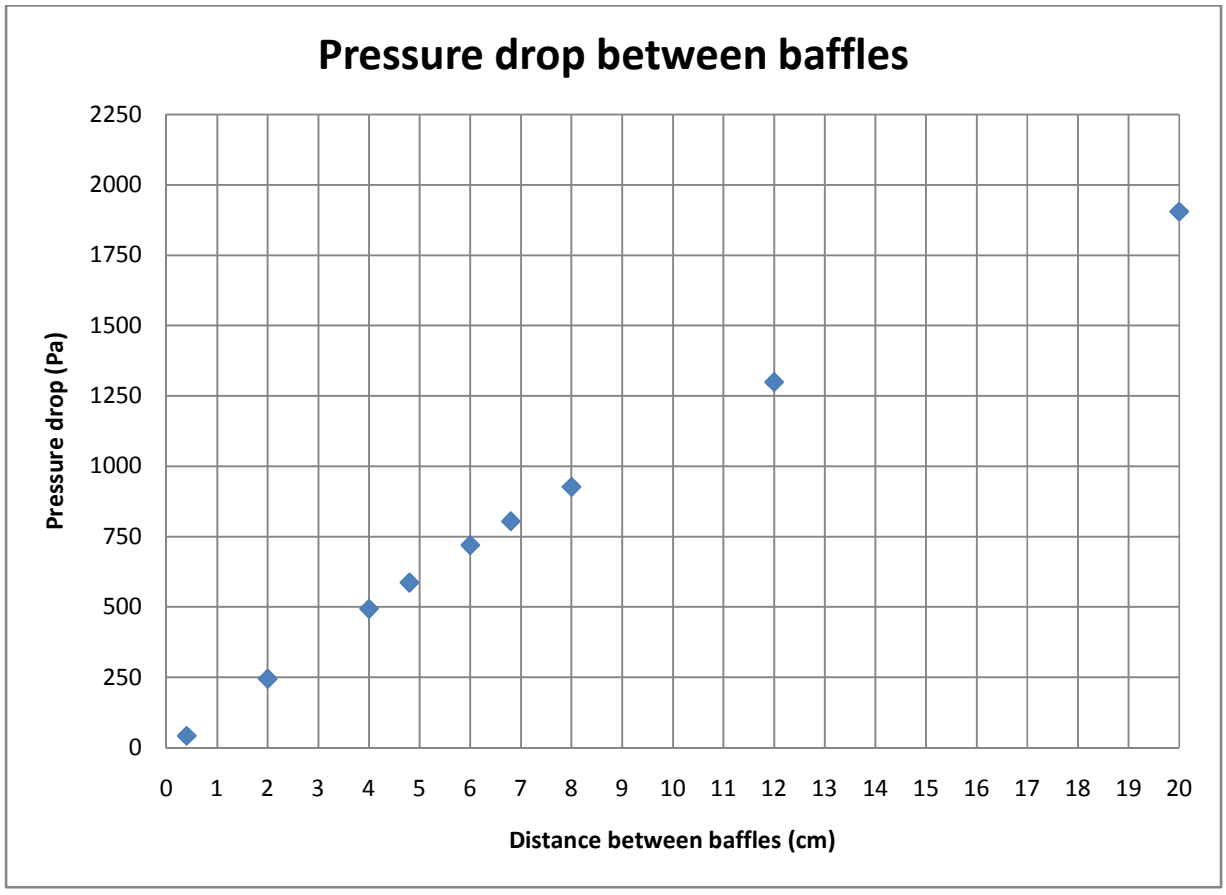

Figure 4.3.1-Pressure drop between baffles

Figure 4.3.1 is a plot of the pressure drop between the end of the first and start of the second baffle; it clearly shows a linear relationship which proves that the flow is following Darcy's law. After 20cm it is possible that the pressure drop stops being a linear relationship due to the channelling becoming significant after this point. Since there is no significant point where pressure increases or decreases from, the optimum distance should primarily be decided on by the average velocity within the channelled region as figure 4.3.2 shows.

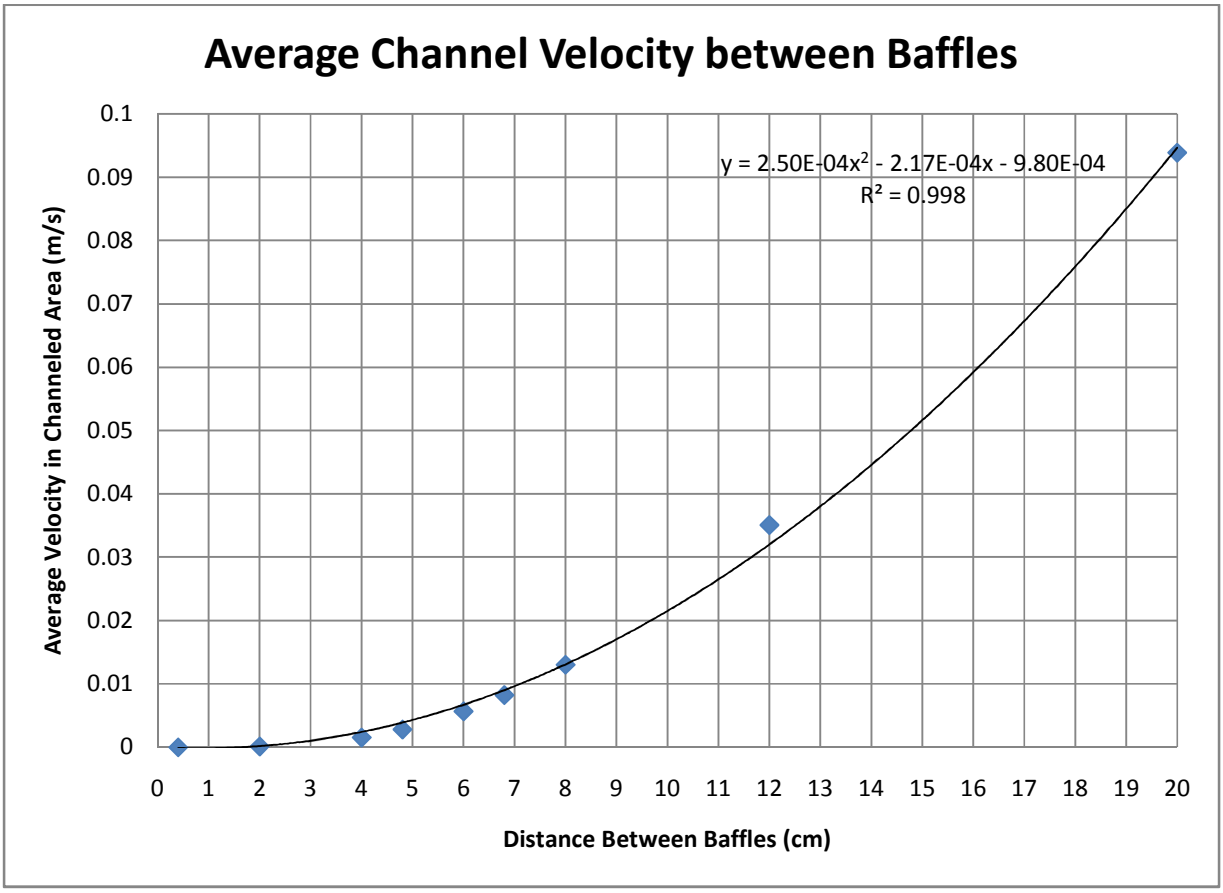

Figure 4.3.2-Average Channel Velocity between Baffles

In the 0 to 20cm region, the average channelled velocity closely follows the polynomial relationship $y = 2.5 \times 10^{-4}x^2 - 2.17 \times 10^{-4}x - 9.8 \times 10^{-4}$ as shown above. While it is unknown at this point what average channel velocity will still provide filtration effectiveness, placing baffles between 4 & 5cm apart should yield decent results, with average velocities in the channelled area being in the range of 0.002 & 0.004 m/s.

4.4-Optimal Geometry

Geometry (Filename: 554-2005-2110)

The optimal geometry model was designed taking figures 4.3.1 & 4.3.2 into account. The baffles are 4.5cm apart, 50mm deep and 2mm wide. The mesh contains approximately 1.2 million nodes and is refined within the area of the baffles.

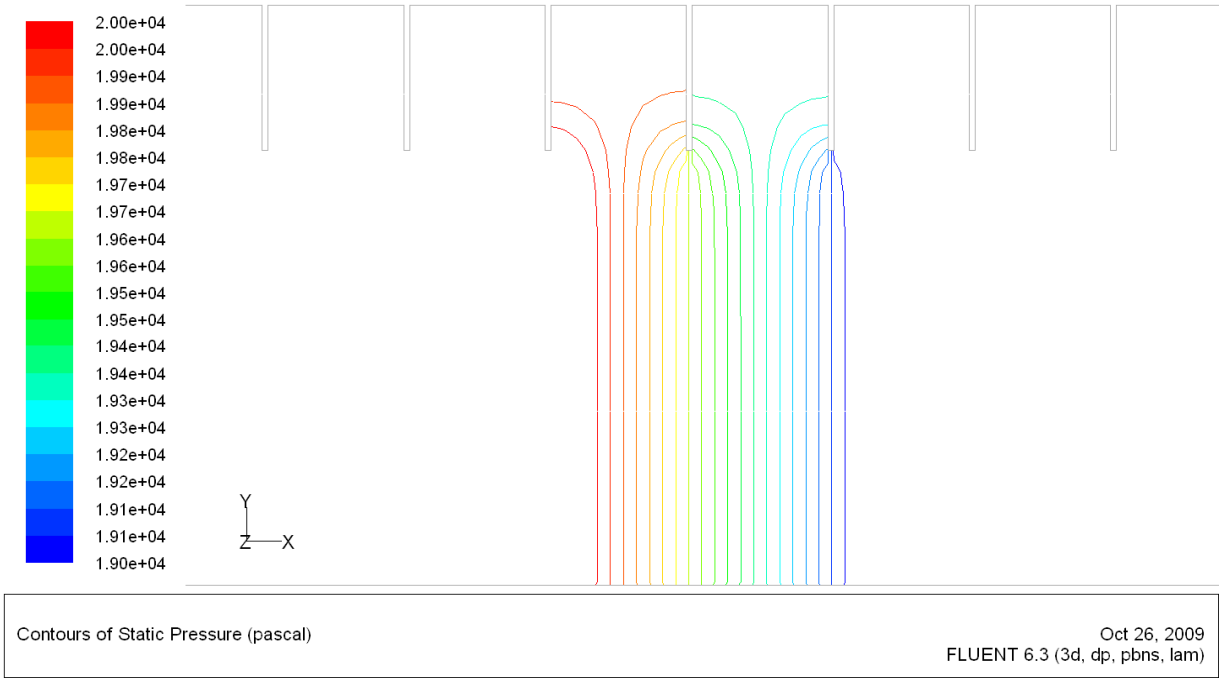

Figure 4.4.1-Pressure contours across optimal geometry baffles (1kPa Range)

The total pressure drop across a 2.5m section of this geometry is 28.95kPa, this suggests that most of the fluid is travelling through the sand as Darcy's law calculates the pressure drop to be around 29kPa for the same effective area[6]. The pressure drop across a baffle is 543Pa, which is considerably less than the pressure drop across previous geometries, because no fluid is flowing through the channelled area as shown in figure 4.4.2. Additionally, the vector plot shows that there is very little fluid flow above the baffles with a fairly even flow below the baffles.

[6] The actual area that the fluid flows through as dictated by the conservation of mass, in this case the area underneath the baffle.

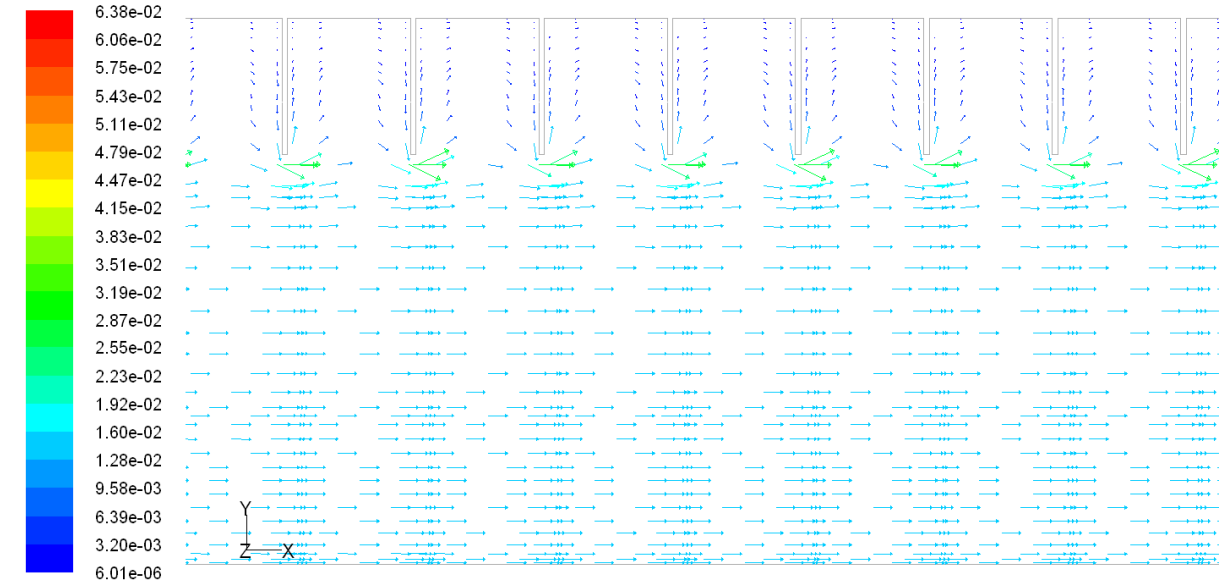

Figure 4.4.2-Velocity Vectors in Optimal Geometry

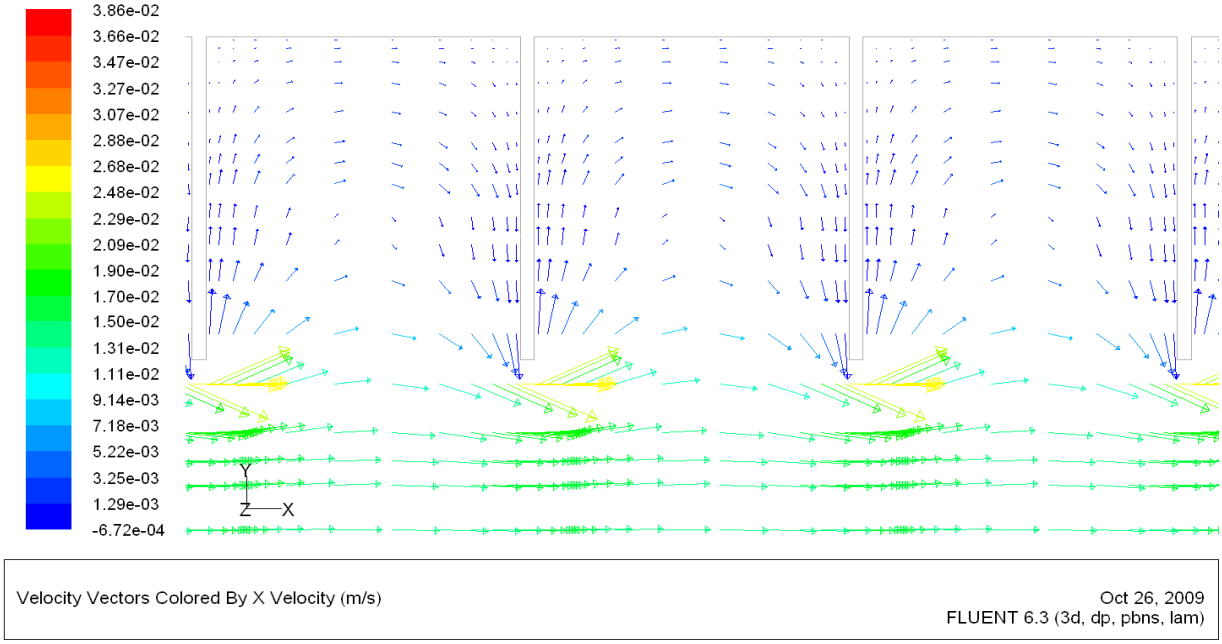

Figure4.4.3-Velocity Vectors in the x direction between baffles in Optimal Geometry

Figure 4.4.3 shows how the fluid travels above the baffles slightly but never reaches any significant velocity in the channelled area, this is reinforced by figure 4.4.4 below which shows that the maximum velocity in the channelled area as 3.3×10^{-3}m/s.

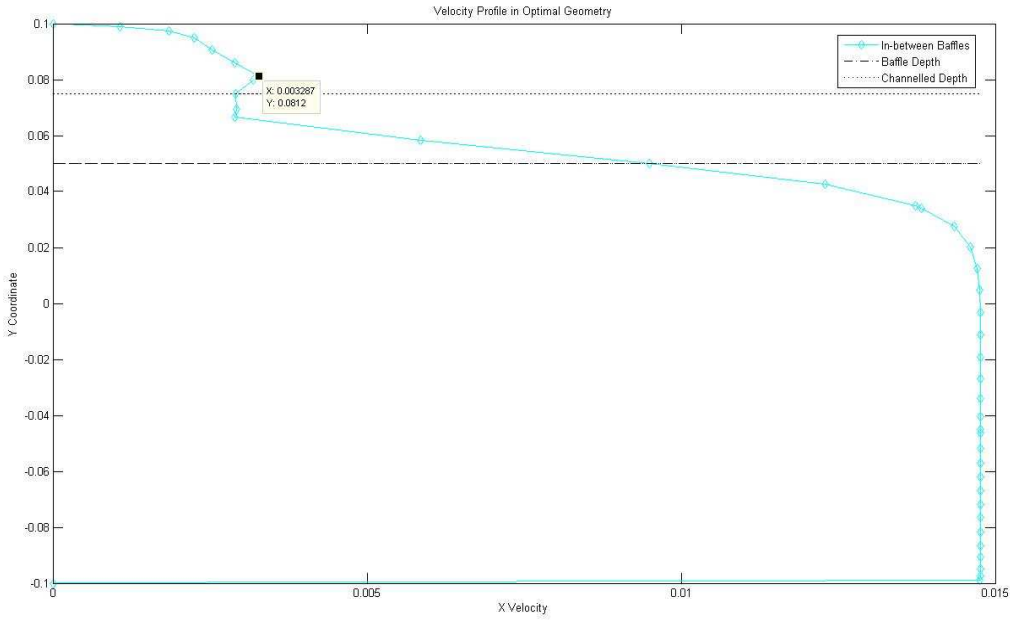

Figure 4.4.4-Velocity Profile in Optimal Geometry

Mesh Convergence

In order to determine the accuracy of the result, a finer mesh was created to ensure that the solution was sufficiently accurate by analysing the convergence of the two meshes. This mesh has approximately 1.4 million nodes and was slightly finer in all areas of the grid compared to the initial mesh.

The key parameters of X velocity, total pressure difference and pressure drop across the baffle and the velocity profiles in between baffles were studied.

	Original Mesh	**Refined Mesh**	**Deviation**
Total Pressure Difference (kPa)	28.95	28.89	0.21%
Pressure Drop Across Baffle (Pa)	543	542	0.18%
Maximum X Velocity (m/s)	3.78E-02	3.77E-02	0.26%

Table 4.4.1-Convergence Study Results

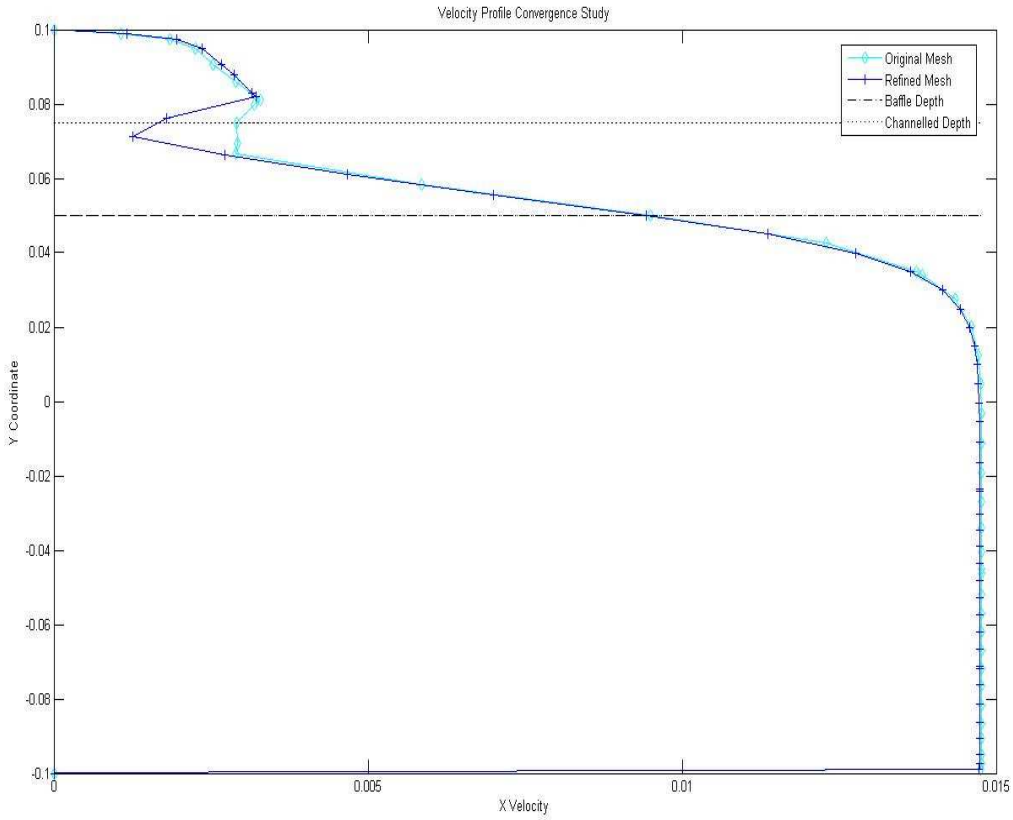

Figure 4.4.5-Convergence Study of Velocity Profiles in between baffles

As the above table and figure shows, there is very little deviation in the key parameters between the two meshes, the only major difference being in a small section of the velocity profile which is relatively insignificant due to the overall low magnitude of the velocity and the local maximum velocity in the channelled area is still the same.

Chapter 5-Experimental Results and Discussion

5.2-Permeability Test

Testing of the permeability of the sand to be used in the validation experiment was done at the USQ Hydraulics Laboratory in August 2009. The sand used was sourced from Riversands Australia and was discussed previously in chapter 3. The results are shown below[7]:

SAND
HEIGHT 0.925 m **AREA** 7.85E-03
WATER
HEIGHT 0.962 m

RUN	TIME (s)	VOLUME (m^3)	FLOWRATE (m^3/s)	VISCOUS RESISTANCE	PERMEABILITY
1	182	0.00315	1.728E-05	4.63E+09	2.16E-10
2	266	0.00452	1.699E-05	4.71E+09	2.12E-10
3	191	0.00332	1.737E-05	4.61E+09	2.17E-10
4	170	0.00292	1.718E-05	4.66E+09	2.15E-10
5	80	0.0014	1.750E-05	4.57E+09	2.19E-10
6	100	0.00172	1.721E-05	4.65E+09	2.15E-10
			AVERAGE	**4.64E+09**	**2.16E-10**
			STD DEV	**4.68E+07**	

Table 5.2.1-Permeability Test Results

[7] Refer to section 3.5.2 for an overview on how the values were calculated

The low variability in these results prove that the flow through the sand was saturated and the deviation of 1% proves that all assumptions are correct and the sand used is homogenous enough to carry out further validation on the numerical model.

The experimental viscous resistance value differs to the viscous resistance value used in the numerical model by about 3×10^{-9} however the permeability should only affect the pressure difference according to Darcy's law so the optimum geometry and method for determining it is still valid.

5.3-Complete System Validation

Validation of the complete system was done at the USQ Hydraulics Laboratory in September and October 2009. A dye was used to visualise the flow through the filter and this was filmed for further investigation. A copy of the film is provided in appendix G.

5.3.1-Numerical Models

Two meshes that represent the complete system were used to check for the convergence of results between the validation and numerical models. Table 5.3.1 shows the statistics for both meshes.

	Grid A	Grid B
Nodes	217 415	1 017 525
Cells	204 425	974 700
Faces	626 004	2 966 214

Table 5.3.1-Grid Statistics for both numerical validation models

Both of these grids model the 1.25m section of the filter combined with the baffles. Both models were solved using the same solver options as used in the optimisation of the numerical model and boundary conditions that represented the validation model. Detailed meshes of these two models are provided in Appendix C.

5.3.2-Results

Due to issues with the selection of the wrong flowmeter, testing of the complete system was done at a constant head of 1.07 metres and the flow rates were determined using the same approach as in the permeability test in order to calculate the inlet velocity which will be used in the numerical model. Table 5.2.2 shows the averaged velocity based on flowrate measurements.

RUN	TIME (s)	VOLUME	FLOWRATE	VELOCITY
1	360	0.00194	5.39E-06	6.34E-04
2	298	0.00158	5.30E-06	6.24E-04
3	570	0.003	5.26E-06	6.20E-04
		AVERAGE	5.32E-06	**6.26E-04**

Table 5.3.2-Average Inlet Velocity for complete system

Pressure

Pressure values were taken on the validation model and both numerical models to check for the convergence of results. Table 5.2.3 shows the pressure difference values for each case.

			Δp (Pa)		
	Manometers	**Δh (m)**	**Model**	**Grid A**	**Grid B**
Overall Filter Length	1-4	0.261	2557.85	2443.89	2563.75
Between Baffles	2-3	0.053	519.41	452.42	513

Table 5.3.3-Pressure Difference Values for experimental and numerical models

The difference in pressure values for grid B are below the maximum pressure error reading and therefore the model can be considered completely validated for that mesh. Table 5.3.4 displays the error percentage for both grids.

	Grid A		**Grid B**	
	|S-D|	**% Error**	**|S-D|**	**% Error**
Overall Filter Length	113.96	4.46%	5.9	0.23%
Between Baffles	66.99	12.90%	6	1.16%

Table 5.3.4-Error Percentage between numerical and experimental models

As can be seen, the pressure error across the entire baffle is less than 5% which is acceptable for validation in this case due to the variability of some of the inputs, especially the permeability of sand. In between the baffles, the pressure error is approximately 13%. While this value is slightly higher than what would be desirable, most of the numerical model meshes are finer than grid A and as the values for grid B show, the error drops off significantly at higher mesh quality.

Most of the numerical mesh spacing's lie between the Grid A and Grid B and therefore the numerical model results can be considered valid for determining an optimal geometry given the level of uncertainty for other values such as permeability. If lower uncertainty levels are required, the results suggest uncertainty would decrease further for finer meshes at the expense of computing time.

Velocity

Velocity values were taken at the outlet of the validation and numerical models. The velocities in the validation model were taken by measurement of the difference between static and stagnation pressures using the pitot tube. The difference between the static and stagnation pressure is called the dynamic pressure and this value was used to compare results between the numerical and validation models.

However due to the low initial velocities, the dynamic pressure was too low to be measured with current equipment and the measurement errors were responsible for most of the measured value. In addition, the screen that was used to hold the sand in place in the filter has the effect of evening out the velocity profiles by an unquantifiable amount, making it difficult to determine the actual velocity values. For these two reasons, the velocity values cannot be considered to be validated using this experimental setup and alternative experiments would need to be conducted to accurately validate these values if it is needed at a future date.

5.3.3-Observations

An additional benefit of modelling the complete system was that observations on how the filter works in practice could be made. This helps refine the numerical model and identify issues for investigation that cannot be identified using the numerical model. A food dye was injected into the model for flow visualisation and was filmed[8] to allow for further investigation if needed. Several key observations were made relating to the variation of the sand properties, the height of the non-porous channel and air bubbles that become trapped in the system.

Upon filling the filter for the first time with dry sand it was observed that the water immediately followed a path that took it along the top of the filter instead of gradually filling the entire filter. Additionally when the filter was completely saturated, the channelled height was different for each segment[9] of the filter with channelled depths of around 8mm in the first segment and 2mm in the last segment.

From this observation it was concluded that the permeability and porosity of the sand are not constant throughout the media and instead vary with the depth of the sand and pressure. The major implication of this observation is that the height of the channelled area varies with the pressure. This variation needs to be taken into account when determining baffle depths so that channelling doesn't occur underneath the baffles. More detailed investigation into this area needs to be carried out however from the observations it was decided that the baffle depth should not be any shorter than ¼ of the pipe diameter.

Another key observation that came from the complete system model is the impact air bubbles trapped in the filter have on the flow. For validation, the filter was first filled vertically and rotated in order to remove all the air bubbles however this process is not viable in an industrial application. Observations showed that the air bubbles tended to be located around the baffles which provided the benefit of forcing the water to travel through more of the sand however

[8] The film is available in appendix G
[9] A segment is considered to be the volume between two baffles

the unpredictability in the formation of these air bubbles means that they need to be removed from the filter by the addition of valves near each baffle.

5.4-Summary

The permeability calculation and complete system validation experiments validated the numerical models used to obtain the optimal geometry to a satisfactory level even though the velocity measurements could not be accurately validated due to the presence of errors that were larger than the recorded results. This is because similarity of the velocity results between the numerical and validation models suggest that the numerical model is acceptable especially when considering the low uncertainty levels in the recorded pressure values.

In addition to the validation, the observations taken from the complete system model can be combined with the numerically determined optimal geometry model to develop a viable geometry that can be used to effectively filter wastewater.

Chapter 6-Discussion

6.1-Filtration Effectiveness and Optimal Geometry

In chapter 4, an optimal geometry was presented based on minimising the fluid velocity in the channelled section of the sand filter in order to produce an effective filter. The inlet velocity of the optimal geometry was varied in order to determine the validity of the optimal geometry.

Three inlet velocities of 0.002, 0.005 and 0.01 m/s were modelled and the velocity profiles are shown in figure 6.1.1.

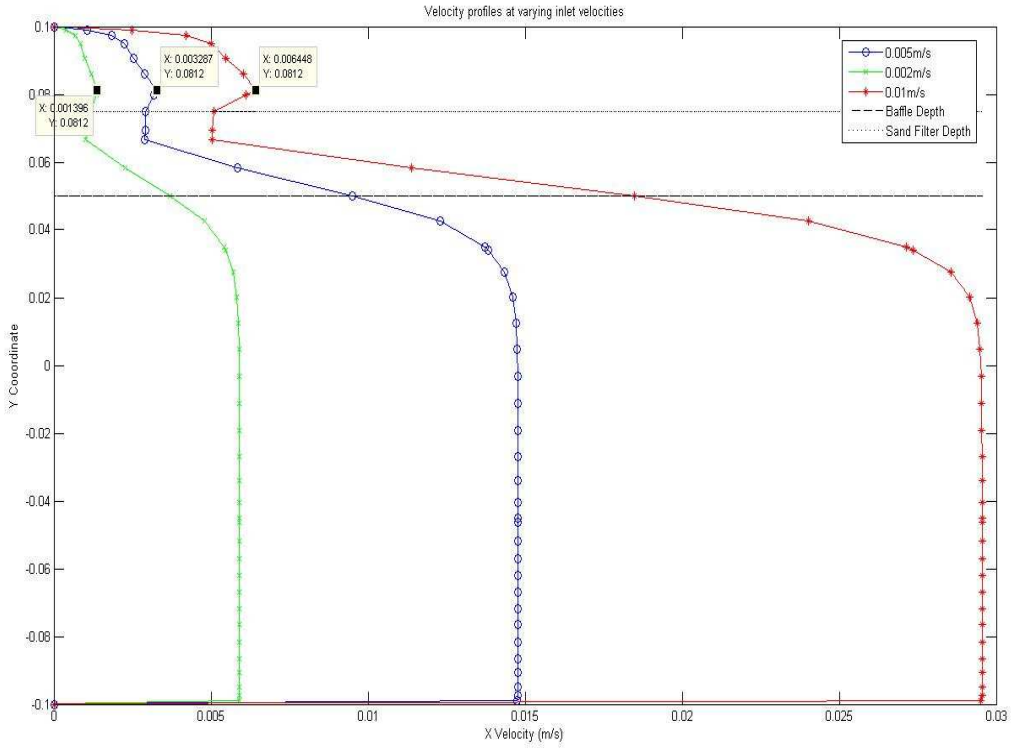

Figure 6.1.1-Velocity Profiles at varying Inlet Velocities

For all three cases the ratio of 1:0.65:3 exists between the inlet velocity, peak channelled and velocity the peak velocity below the baffle. This indicates that the velocity profile holds a

specific ratio regardless of the inlet velocity[10]. Similar ratios should also exist for geometries with different baffle spacing's.

This geometric ratio is extremely useful in designing the geometry of filters since the filtration effectiveness is a function of the velocity profile. For example, if filter length is not an issue, a geometry with a lower filter effectiveness per unit length could be used. The baffle spacing's could be determined by estimating the velocity profile ratio which corresponds to the specific geometry.

[10] While it is unproven, it is safe to assume this only occurs in laminar flow.

Chapter 7-Conclusions and Future Work

7.1-Optimal Configuration

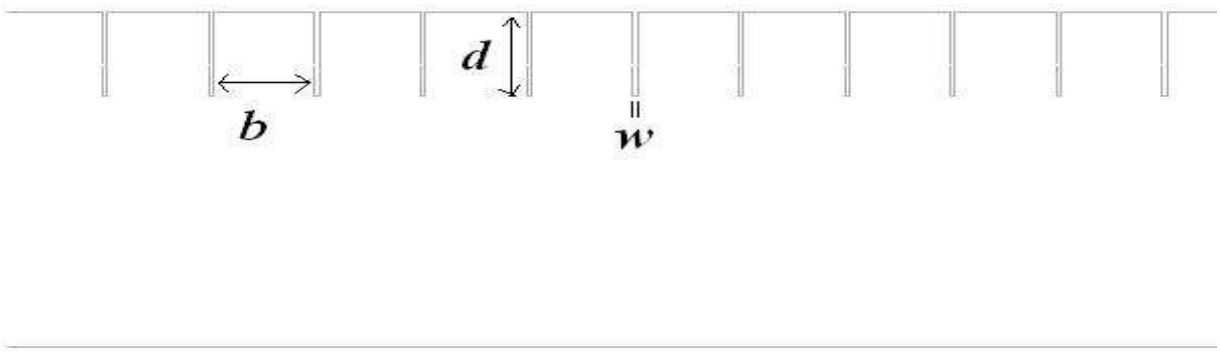

Figure 7.1.1-Optimal Geometry Configuration for Horizontal Flow Sand Filter

The optimal geometry configuration for the horizontal flow sand filter is shown in Figure 6.1.1. It was derived from numerical modelling results and was validated experimentally. The depth of the baffles was recommended to be at least twice the channel depth *d.* This is due to the effects localised pressure and high velocities creating small channels underneath the baffle. This was observed experimentally.

The baffle width *w* does not have any significant effect on the model because the key principle governing the reason why baffles are ideal is the conservation of mass, it can be as thin as a knife blade as long as it is strong enough to not break under the forces applied to it (pressure, weight of the sand).

For inlet velocities of between 0.002 and 0.01 m/s the optimal baffle spacing *b* in the case of a 0.2m diameter pipe is 4.5cm. More importantly a relationship has been found between the velocity profile and the baffle spacing. This allows for filter designs to be optimised based on targeted filtration effectiveness.

7.2-Significance

The numerical model was validated according to AIAA-G-077 and is valid for all flows that involve the same phenomena and conditions. Other geometries such as a pipe with a spiral protrusion (Mossad & Aral 2009) have similar characteristics to the baffled geometry and the optimal baffle geometry can be used as a starting point to identify the optimal configuration of alternative geometries if required.

The results and process presented in this paper were derived by considering the fluid flow through the filter, with the objective of minimising the velocity of the fluid in the channelled area. No consideration has been given to the effectiveness of the filter at removing impurities. This could mean that the geometry is optimal from a flow perspective only. However, a process of determining the optimal spacing was outlined and can be followed if a minumum velocity within the channelled area is the aim for subsequent filtration effectiveness studies.

7.3-Future Research

From the numerical modelling, experimental observations and review of literature several areas of further research have been identified. This research is required before the concept of the horizontal flow sand filter can be utilised industrially. Further work may involve:

- A study into the effectiveness of the horizontal filter at removing impurities. This research has only developed an optimal geometry from a purely flow perspective. As a result it may not be optimal in terms of filtration effectiveness. Both experimental and numerical analysis would be needed.
- A study into backwashing methods of the filter. Normal vertical filters are usually backwashed every 24 hours to remain efficient. For vertical filters the process is simple as the flow can just be reversed. In order to be competitive with vertical filters, a simple backwashing mechanism needs to be developed for the horizontal filter.

- An accurate comparison between the filtration effectiveness of horizontal and vertical filters. This is important in determining the viability of the horizontal filter in different applications.

- Further development regarding the optimal baffle spacing. It is believed that there is a relationship between baffle depth, permeability, channel depth and the optimal spacing. Numerical investigations to list the direct relationships of optimal baffle spacing's would be beneficial in designing horizontal sand filters.

Chapter 7-References

American Institute of Aeronautics and Astronautics 1998, *Guide for the Verification and Validation of Computational Fluid Dynamics Simulations (AIAA-G-077-1998)*, AIAA Standards.

American Water Works Association, 2007, *Reverse Osmosis and Nanofiltration*, 2nd edn, American Water Works Association, Denver, USA.

Binnie, C, Kimber, M & Smethurst, G 2002, *Basic Water Treatment*, 3rd edn, Thomas Telford, London.

Chung, CA 2003, *Simulation Modeling Handbook: A practical Approach,* CRC Press, Florida.

Darcy, H. 1856, *Les Fontains Publiques dela Ville de Dijon.* Victor Dalmont, Paris.

du Plessis, P, Diedericks, G. 1997, *Fluid Transport in Porous Media*, Computational Mechanics Publications, Bath, United Kingdom.

Fox, RW, Pritchard, PJ & McDonald, AT 2008, *Introduction to Fluid Mechanics*, 7th edn, John Wiley & Sons, USA.

Freeze, R 1994, '*Henry Darcy and the Fountains of Dijon*' Ground Water, vol. 32, no. 1, pp. 23-30.

Hammer, M & Hammer, M Jr. 1986, *Water and Wastewater Technology*, 3rd edn, Prentice Hall, Upper Saddle River, New Jersey.

Havard, P, Jamieson, R, Cudmore, D, Boutilier, L & Gordon, R 2008, 'Performance and Hydraulics of Lateral Flow Sand Filters of On-Site Wastewater Treatment' Journal of Hydrologic Engineering, vol. 13, no. 8, pp. 720-728.

Horváth, I 1994, *Hydraulics in water and Waste-Water Treatment Technology*, John Wiley & Sons, West Sussex.

Katsaounis, T & Levy, D 1999, 'A Modified Structured Central Scheme for 2D Hyperbolic Conservation Laws' *Applied Mathematics Letters*, vol. 12, 1999, pp. 89-96.

Kawamura, S 2000, *Integraded design and Operation of Water Treatment Facilities*, 2nd edn, John Wiley & Sons, Canada.

Mossad, R & Aral, A 2009, 'Numerical Modelling of Horizontal Flow in a Porous Sand Media'

Natare Corporation, 2003, 'Filter Media (Sand) Typical Specification' Technical Data and Engineering Notes, Available from www.natare.com.

Rowe, D, Abdel-Magid, I. 1995, *Handbook of Wastewater Reclamation and Reuse*, CRC Press, Boca Raton, Florida.

Scheidegger, A. 1960, *The Physics of Flow through Porous Media*, University of Toronto Press, Bath, United Kingdom.

Stern, F, Wilson RV, Coleman, HW & Paterson, EG 2001, 'Comprehensive Approach to Verification and Validation of CFD Simulations-Part 1: Methodology and Procedures' *Journal of Fluids Engineering*, vol. 123, December 2001, pp. 793-802.

Vafai, K 2000 *Handbook of Porous Media*. CRC Press, Florida.

Venkataraman, P, Rao, P, 1998, 'Darcian, Transitional, and Turbulent Flow through Porous Media' *Journal of Hydraulic Engineering*, vol. 124, no. 8, pp. 840-846

Ward, J, 1964, 'Turbulent Flow in Porous Media' *Journal of the Hydraulics Division*, vol. 90, no. 5, pp. 1-12

Appendix A-Project Specification

FOR: **Stuart MEAD**

TOPIC: Numerical Modelling of Horizontal Flow in a Sand Filter

SUPERVISOR: Dr Ruth Mossad
Dr Hal Aral
CSIRO Minerals, Clayton Vic.

SPONSORHSIP: Faculty of Engineering & Surveying/Some contribution from CSIRO

PROJECT AIM: To use computational fluid dynamics software to investigate the water flow dynamics of a horizontally laid sand filter in order to determine an optimum configuration for the horizontal column (shown in attachment A) that will reduce the effect of channelling that occurs.

PROGRAMME: (**Issue B, 20/10/2009**)

1. Research the background information relating to flow through porous media, current filtration methods and strategies to prevent channelling.

2. Learn how to use computational fluid dynamics (CFD) software Fluent.

3. Apply the Fluent software to investigate the flow through a horizontal column with the baffled pipe geometry as shown in attachment A.

4. Determine an optimum configuration for the horizontal column by altering the size, shape and position of the baffles shown in attachment A so that water sweeps the entire column with minimal channelling.

5. Investigate the effects of altering the porosity of the sand in the column to minimise channelling.

As time permits:

6. Investigate alternate geometries that may minimise channelling in a horizontal filter.

7. Validate the findings of the CFD software through lab experiments.

AGREED _____ (student) _____ (supervisors)

Date: 28 /10/ 2009 Date: 28/10/2009

Assistant Examiner: _____

University of Southern Queensland

FACULTY OF ENGINEERING AND SURVEYING

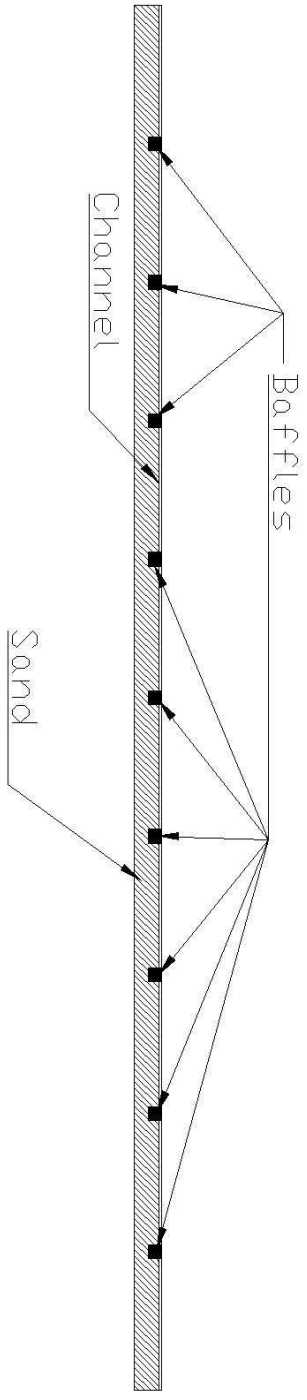

Appendix B-UDF

```
/* Viscous Resistance Profile UDF in a Porous Zone that utilizes F_PROFILE*/

/*Baffleproper*/

/*Volume 0.311332 0.02 length*/

#include "udf.h"

DEFINE_PROFILE(vis_res,t,i)

{

real y[ND_ND];

real a;

cell_t c;

begin_c_loop(c,t)

{

C_CENTROID( y,c,t);

if( y[1] < 0.081 )

a = 1.95e9;

else

a = 1e6;

F_PROFILE(c,t,i) = a;

}

end_c_loop(c,t)

}
```

Appendix C-Detailed Meshes

C.1-Geometry 1

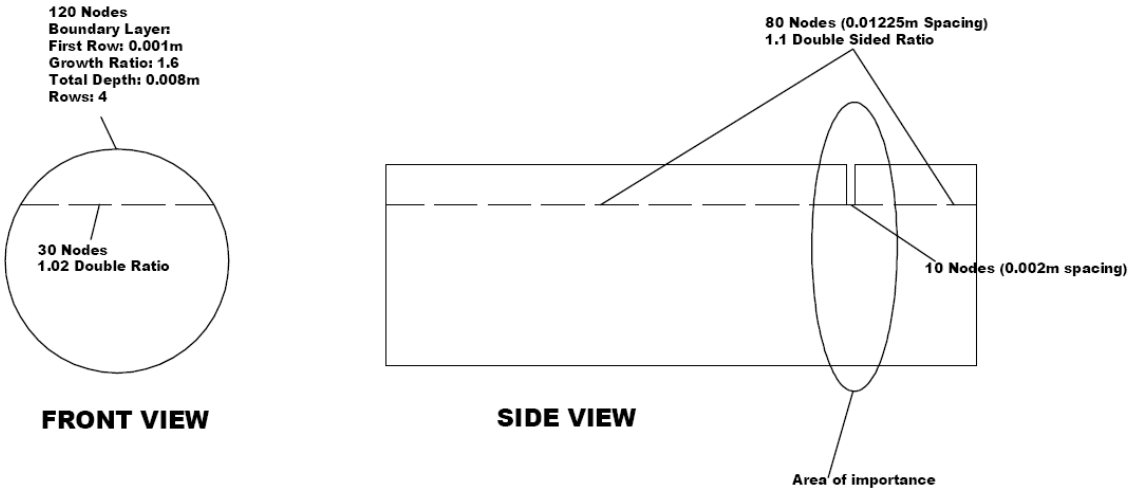

Figure C.1 -Meshing Scheme for Geometry 1

File Name	111-205-2707
Nodes	1 083 213
Cells	3 129 087
Faces	1 023 480

Table C.1 -Grid Information for Geometry 1

C.2-Geometry 2

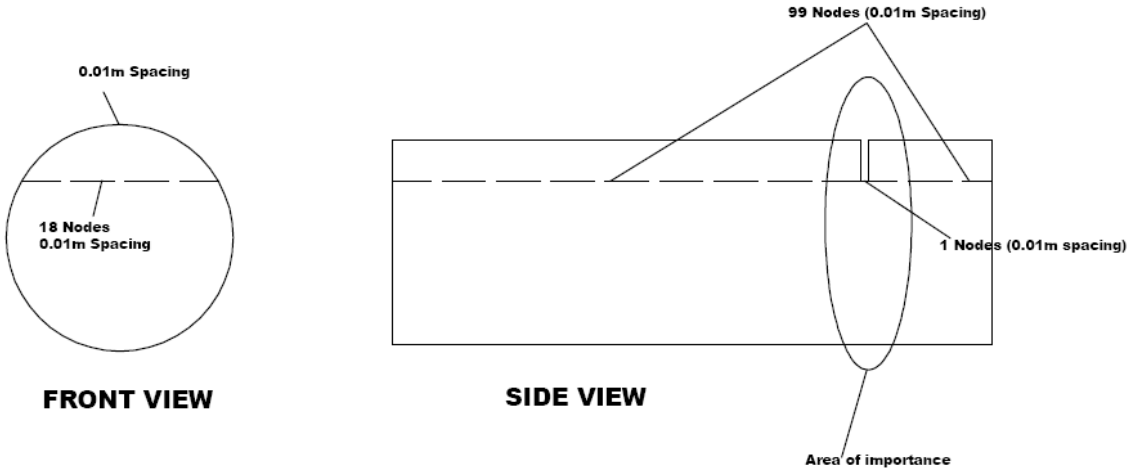

Figure C.2 -Meshing Scheme for Geometry 2

File Name	555-205-2307
Nodes	353 796
Cells	319 920
Faces	992 585

Table C.2 -Grid Information for Geometry 2

C.3-Geometry 2a

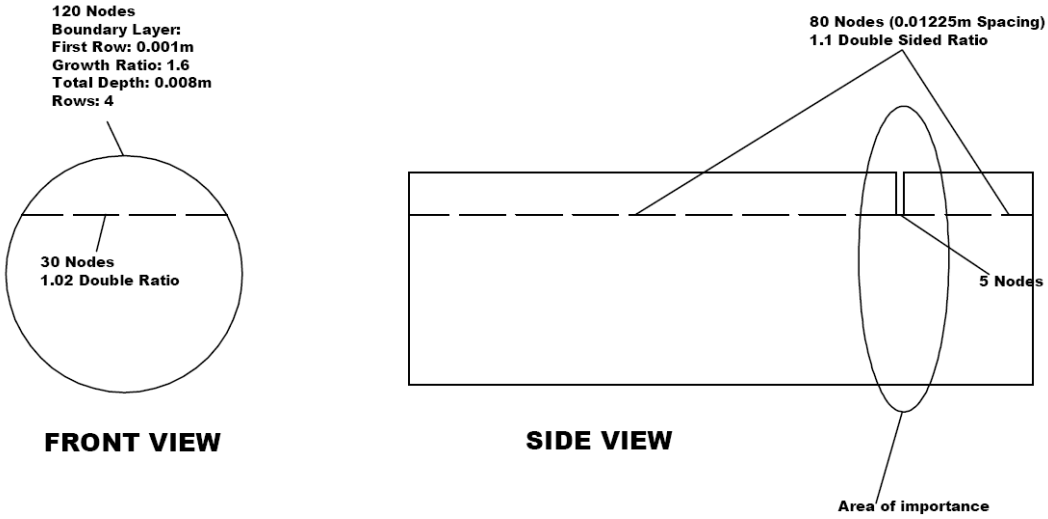

Figure C.3 -Meshing Scheme for Geometry 2a

File Name	555-205-2707
Nodes	1 409 084
Cells	1 343 210
Faces	4 094 448

Table C.3 -Grid Information for Geometry 2a

C.4-Geometry 3

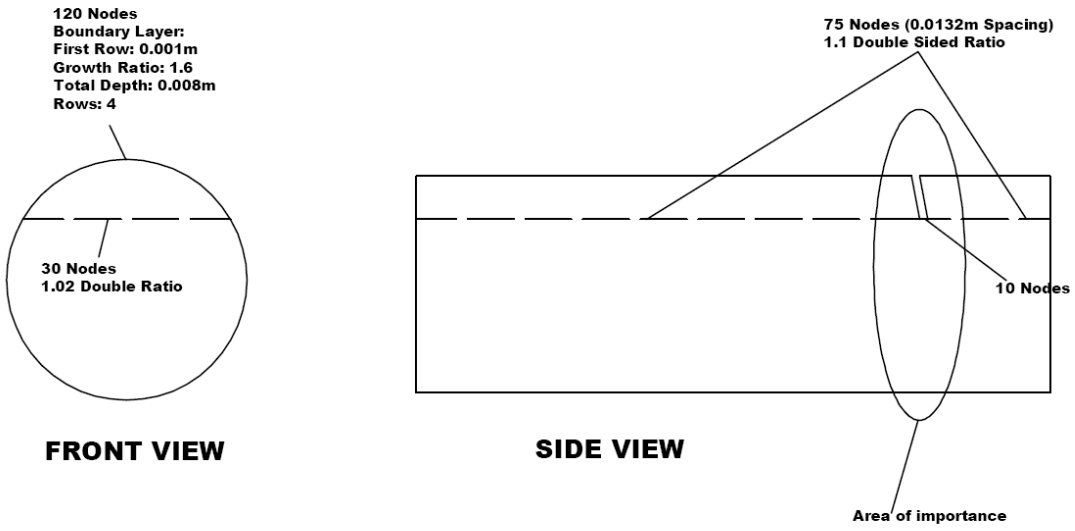

Figure C.4 -Meshing Scheme for Geometry 3

File Name	551-205-2707
Nodes	1 234 713
Cells	1 179 645
Faces	3 593 057

Table C.4 -Grid Information for Geometry 3

C.5-Geometry 4

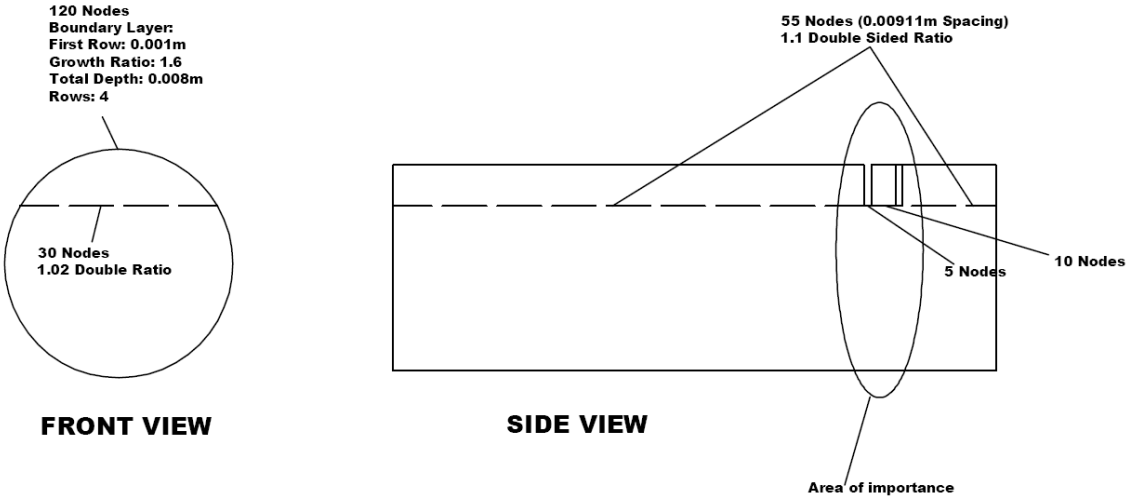

Figure C.5 -Meshing Scheme for Geometry 4

File Name	556-2005-2707
Nodes	1 236 655
Cells	1 190 840
Faces	3 6187 654

Table C.5 -Grid Information for Geometry 4

C.6-Geometry 5

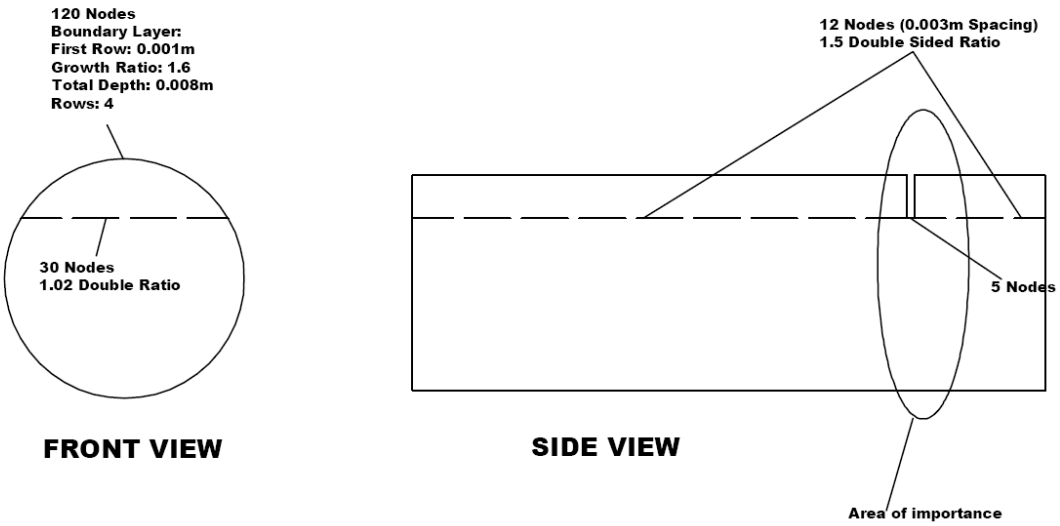

Figure C.6 -Meshing Scheme for Geometry 5

File Name	754-2005-0308
Nodes	1 236 655
Cells	1 190 840
Faces	3 187 654

Table C.6 -Grid Information for Geometry 5

C.7-Optimal Geometry

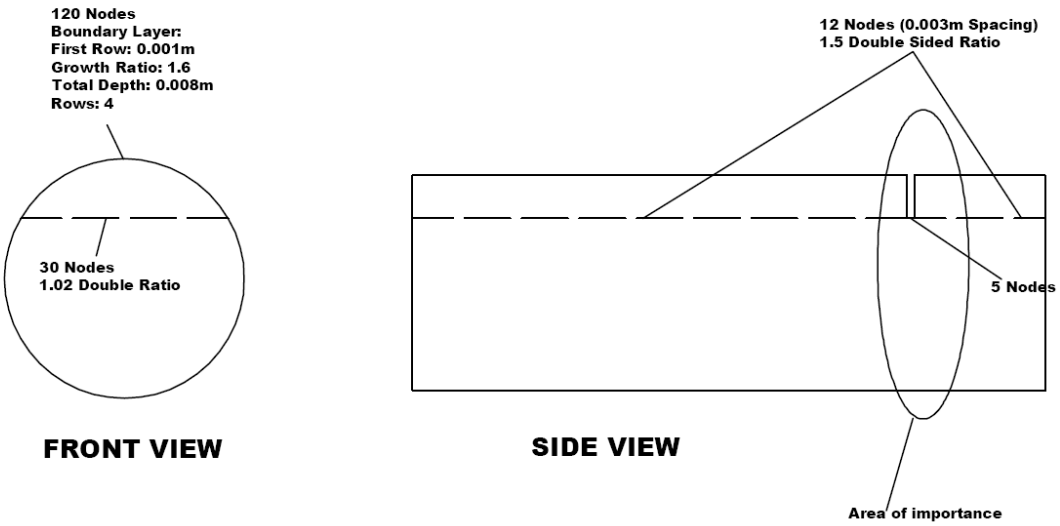

Figure C.7 -Meshing Scheme for Optimal Geometry

File Name	554-2005-2110
Nodes	1 210 651
Cells	1 140 328
Faces	3 490 090

Table C.7 -Grid Information for Optimal Geometry

C.8-Optimal Geometry Refined Mesh

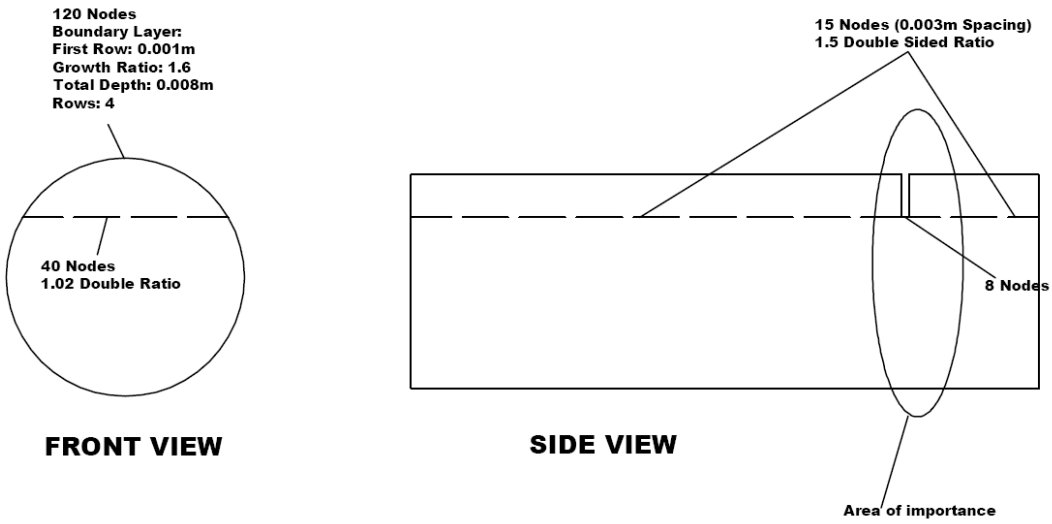

Figure C.8 -Meshing Scheme for Optimal Geometry Refined Mesh

File Name	554-B
Nodes	1 210 651
Cells	1 140 328
Faces	3 490 090

Table C.8 -Grid Information for Optimal Geometry Refined Mesh

C.9-Validation Model Mesh

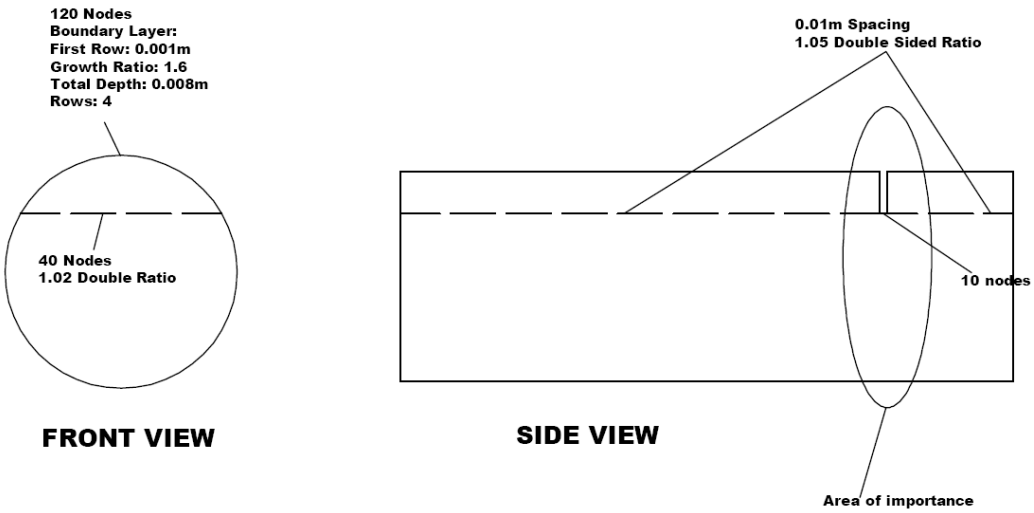

Figure C.9 -Meshing Scheme for Validation Model Mesh

File Name	Valexp-3.3.1
Nodes	217 415
Cells	204 425
Faces	626 004

Table C.9 -Grid Information for Validation Model Mesh

C.10-Validation Model Refined Mesh

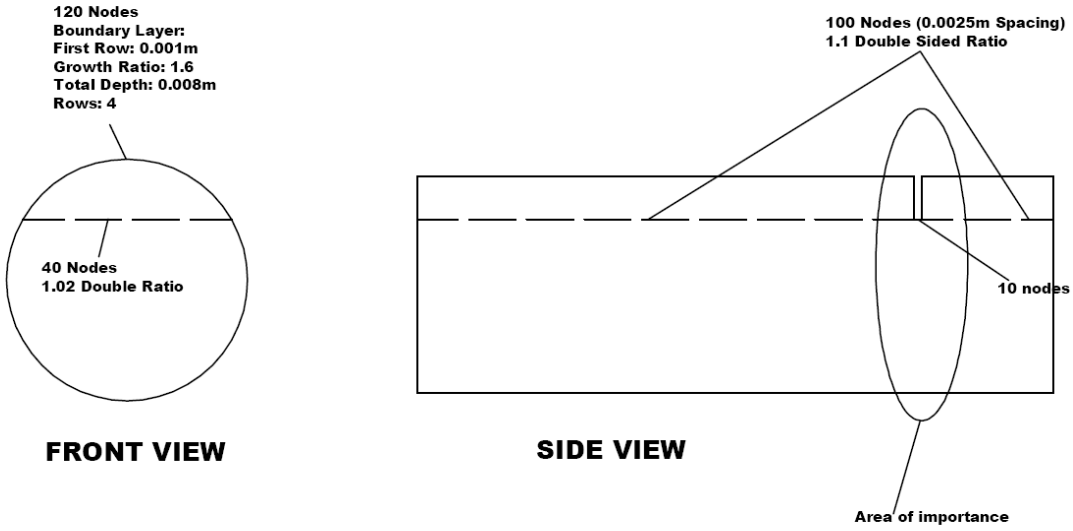

Figure C.10 -Meshing Scheme for Validation Model Refined Mesh

File Name	valexp
Nodes	1 017 525
Cells	974 700
Faces	2 966 214

Table C.10 -Grid Information for Validation Model Refined Mesh

Appendix D-Chord Calculations

Area	Small Radius	Area	Small Radius	Area	Small Radius
0.015508	0.001	0.0084805	0.037	0.0025356	0.073
0.015308	0.002	0.0082951	0.038	0.0024	0.074
0.015108	0.003	0.0081105	0.039	0.0022666	0.075
0.014908	0.004	0.0079267	0.04	0.0021354	0.076
0.014708	0.005	0.0077439	0.041	0.0020066	0.077
0.014509	0.006	0.0075619	0.042	0.0018802	0.078
0.014309	0.007	0.0073809	0.043	0.0017563	0.079
0.01411	0.008	0.0072008	0.044	0.001635	0.08
0.01391	0.009	0.0070217	0.045	0.0015164	0.081
0.013711	0.01	0.0068436	0.046	0.0014005	0.082
0.013512	0.011	0.0066665	0.047	0.0012875	0.083
0.013314	0.012	0.0064905	0.048	0.0011774	0.084
0.013115	0.013	0.0063156	0.049	0.0010705	0.085
0.012917	0.014	0.0061418	0.05	0.00096674	0.086
0.012719	0.015	0.0059692	0.051	0.00086639	0.087
0.012522	0.016	0.0057978	0.052	0.00076957	0.088
0.012324	0.017	0.0056276	0.053	0.00067646	0.089
0.012127	0.018	0.0054586	0.054	0.00058726	0.09
0.011931	0.019	0.0052909	0.055	0.00050219	0.091
0.011735	0.02	0.0051245	0.056	0.00042151	0.092
0.011539	0.021	0.0049595	0.057	0.00034553	0.093
0.011344	0.022	0.0047959	0.058	0.00027462	0.094
0.011149	0.023	0.0046337	0.059	0.00020923	0.095
0.010954	0.024	0.004473	0.06	0.00014994	0.096
0.010761	0.025	0.0043137	0.061	9.75E-05	0.097
0.010567	0.026	0.004156	0.062	5.32E-05	0.098
0.010374	0.027	0.0039999	0.063	1.88E-05	0.099
0.010182	0.028	0.0038454	0.064		
0.0099903	0.029	0.0036925	0.065		
0.0097992	0.03	0.0035414	0.066		
0.0096087	0.031	0.0033921	0.067		
0.0094189	0.032	0.0032445	0.068		
0.0092298	0.033	0.0030988	0.069		
0.0090413	0.034	0.002955	0.07		
0.0088536	0.035	0.0028131	0.071		
0.0086667	0.036	0.0026733	0.072		

Appendix E-Experiment Setup

F1-Complete System Model

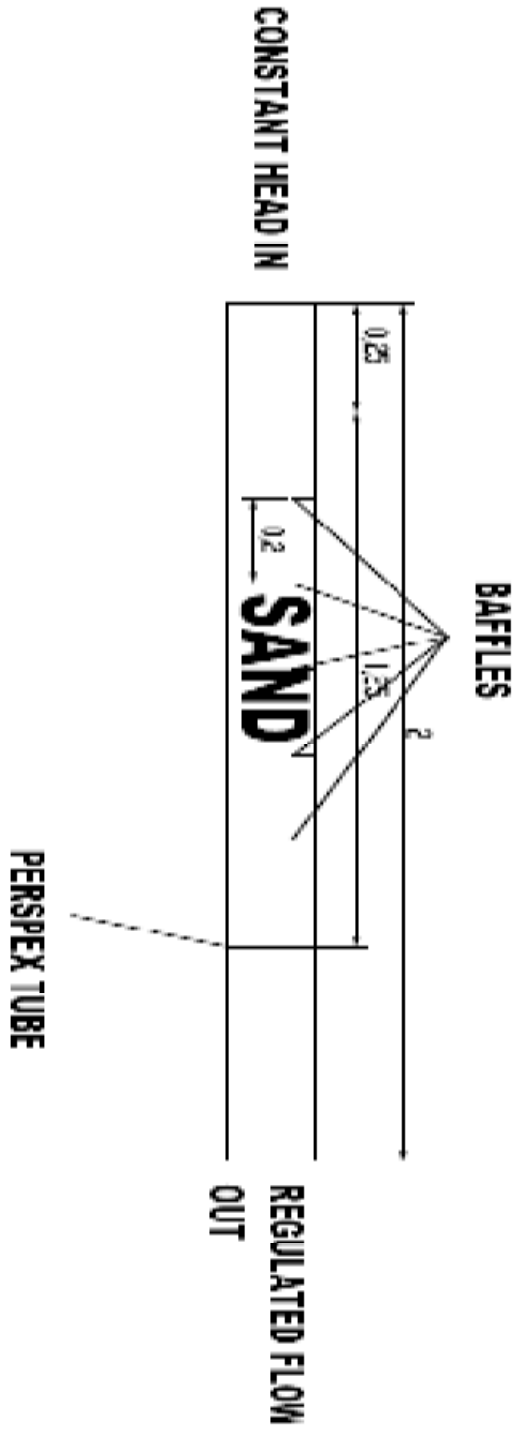

Appendix F-Experimental Equipment Data Sheets

F.1-Pitot Tube Data Sheet

Bulletin H-11

Series 160 Stainless Steel Pitot Tubes

Specifications - Installation and Operating Instructions

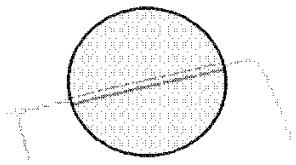

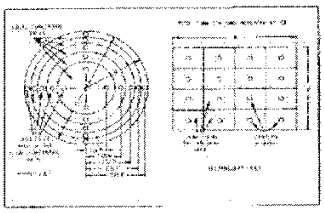

The total pressure of an air stream flowing in a duct is the sum of the static or bursting pressure exerted upon the sidewalls of the duct and the impact or velocity pressure of the moving air. Through the use of a pitot tube connected differentially to a manometer, the velocity pressure alone is indicated and the corresponding air velocity determined.

For accuracy of plus or minus 2%, as in laboratory applications, extreme care is required and the following precautions should be observed:

1. Duct diameter to be 30 times pitot tube diameter, or greater.
2. Make an accurate traverse per sketch at right, calculate the velocities and average the readings.
3. Provide smooth, straight duct sections a minimum of 6 1/2 diameters in length upstream and 1 1/2 diameters downstream from the pitot tube.
4. Provide an egg crate type straightener upstream from the pitot tube.

In making an air velocity check select a location as suggested above, connect tubing leads from both pitot tube connections to the manometer and insert in the duct with the tip directed into the air stream. If the manometer shows a minus indication reverse the tubes. With a direct reading manometer, air velocities will now be shown in feet per minute. In other types, the manometer will read velocity pressure in inches of water and the corresponding velocity will be found from the curves in this bulletin. If circumstances do not permit an accurate traverse, center the pitot tube in the duct, determine the center velocity and multiply by a factor of .9 for the approximate average velocity. Field tests run in this manner should be accurate within plus or minus 5%.

The velocity indicated is for dry air at 70°F., 29.9" Barometric Pressure and a resulting density of .075#/cu. ft. For air at a temperature other than 70°F. refer to the curves in this bulletin. For other variations from these conditions, corrections may be based upon the following data:

$$\text{Air Velocity} = 1096.2 \sqrt{\frac{Pv}{D}}$$

where Pv = velocity pressure in inches of water
D = Air density in #/cu. ft.

$$\text{Air Density} = 1.325 \times \frac{P_B}{T}$$

where P_B = Barometric Pressure in inches of mercury
T = Absolute Temperature (indicated temperature °F plus 460)
Flow in cu. ft. per min. = Duct area in square feet x air velocity in ft. per min.

AIR VELOCITY CALCULATOR
Computes velocity based on air density corrected for conditions of temperature and pressure. Eliminates tedious calculations. Ranges from .01 to 10" water corresponding to 400 to 20,000 FPM. Furnished with each pitot tube.

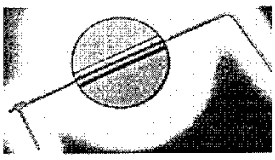

STAINLESS STEEL PITOT TUBES
Test confirmed unity coefficient and lifetime construction of No. 304 stainless steel. Inch graduations show depth of insertion for traversing. Model 160 is designed to meet ASME "Fluid Meters" 6th Ed. ANSI/AMCA 210-99, ANSI/ASHRAE 51-1999, and British Standard 1042. Sizes 12" to 60" long. Hand or fixed mounting types.

DWYER INSTRUMENTS, INC.
P.O. BOX 373 • MICHIGAN CITY, INDIANA 46361, U.S.A.
Phone: 219/879-8000
Fax: 219/872-9057
www.dwyer-inst.com
e-mail: info@dwyer-inst.com

F.2-Flowmeter Data Sheet

Bulletin F-33

Series VF Visi-Float® Flowmeter

Specifications - Installation and Operating Instructions

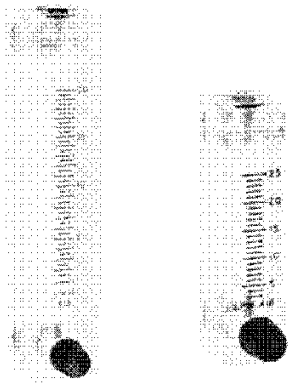

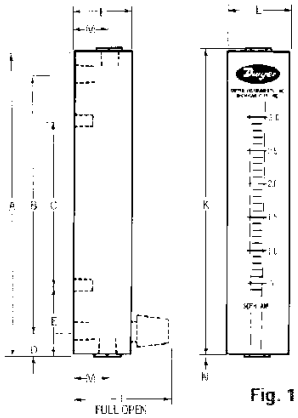

Fig. 1

The Visi-Float® Series Flowmeters are furnished in two models (see Figure 1) each available in a broad choice of flow ranges with direct reading scales for air, gas or water. Installation, operation and maintenance are very simple and only a few common sense precautions must be observed to assure long, trouble free service.

CALIBRATION
Each flowmeter is calibrated at the factory. If at any time during the meter's life, you wish to recheck its calibration, do so only with devices of certified accuracy. **DO NOT** attempt to check the Visi-Float® Flowmeter with a similar flowmeter as seemingly unimportant variations in piping and back pressure may cause noticeable differences in the indicated reading. If in doubt, return your flowmeter to the factory. It will be checked for conformance at no charge. Before proceeding with the installation of your Visi-Float® Flowmeter, check to be sure you have the model and flow range you require.

LOCATION
Temperature, Pressure, Atmosphere, and Vibration:
Visi-Float® Acrylic Flowmeters are exceptionally tough and strong. They are designed for use at pressures up to 100 psig (7 bar) and temperatures up to 150°F (66°C). DO NOT EXCEED THESE LIMITS! The installation should not be exposed to strong chlorine atmospheres or solvents such as benzene, acetone, carbon tetrachloride, etc. The mounting panel should be free of excessive vibration since it may prevent the unit from operating properly.

Inlet Piping Run: It is good practice to approach the flowmeter inlet with as few elbows and restrictions as possible. In every case the inlet piping should be at least as large as the connection to the flowmeter i.e. ¼" Iron Pipe Size. Length of inlet piping makes little difference for normal pressure fed flowmeters.

For flow meters on vacuum air service the inlet piping should be as short and open as possible. This will allow operation near atmospheric pressure and thereby insure the accuracy of the device. (Note that for vacuum air service the flow control valve if any, should be on the discharge side of the flowmeter. Either the TMV unit or a separate in line valve may be applied.)

Discharge Piping: As on the inlet, discharge piping should be at least as large as the flowmeter connection. In addition, for pressure fed flowmeters on air or gas service the discharge piping should be as short and open as possible. This will allow operation of the flow tube at near atmospheric pressure and insure the accuracy of the device. This is of less importance on water or liquid flowmeters, since the flowing medium is generally incompressible and moderate back pressure will not affect the accuracy of the instrument as calibrated.

DIMENSION-IN INCHES		
	Model VFA	Model VFB
A	4	6 ⅛
B	3 (⅛ female NPT)	5⅛ (⅛ female NPT)*
C	1⅛ (10-32 Thread)	3 ⅛ (10-32 thread)
D	⅜	⅜
E	1⅛	1⅛
F	1⅛	1⅛
J	2¼ (BV or SSV)	2¼ (BV or SSV)
K	4⅜	6⅞
L	1	1⅛
M	⅞ (EC)	⅞ (EC)
N	⅝ (EC)	⅝ (EC)

*VFB ranges B5 and B6 have ¼" NPT back connections or ⅜" NPT side connections.

SPECIFICATIONS
Service: Compatible gases & liquids.
Wetted Materials:
Body: Acrylic plastic.
O ring: Buna N (Fluorocelastomer available).
Metal Parts: Brass standard, stainless steel optional.
Float: Stainless steel, black glass, aluminum, K Monel depending on range.
Temperature & Pressure Limits:
Without Valve: 100 psig (6.9 bar) @ 150°F (65°C);
150 psig (10 bar) @ 100°F (38°C).
With Valve: 100 psig (6.9 bar) @ 120°F (48°C).
Accuracy: VFA – 5% of full scale; VFB– 3% of full scale.
Process Connection: 1/8" female NPT. VFB ranges B5 and B6 have 1/4" NPT back connections or 3/8" NPT side connections. These ranges not available with brass valves.
Scale Length: VFA 2" typical length. VFB 4" typical length.
Mounting Orientation: Mount in Vertical Position.
Weight: VFA: 4.0 4.8 oz (.11 .14 kg). VFB: 7.2 8.8 oz (.20 .25 kg).

POSITION AND MOUNTING
All Visi-Float® Flowmeters must be mounted in a vertical position with the inlet connection at the bottom and outlet at the top.

Surface Mounting: Drill appropriate holes in panel using the dimensions shown in Figure 1. Hold the flowmeter in position in front of the panel and install the mounting screws through the panel from the rear. Mounting screws must not be longer than the panel thickness plus ⅛" or the screw will hit the plastic and may damage the meter. The screws will require additional force during the initial installation, since the insert boots are of a collapsed thread type and must be expanded into the plastic for the knurled surface to take hold. Insert boots will not have the proper 10-32 threads

DWYER INSTRUMENTS, INC.
P.O. BOX 373 • MICHIGAN CITY, IN 46361, U.S.A.
Phone: 219/879-8000
Fax: 219/872-9057
www.dwyer-inst.com
e-mail: info@dwyer-inst.com

POPULAR RANGES

Model VFA — 2" Scale			
Range No.	Range SCFH Air	Range No.	Range LPM Air
1	1-1	21	.06-0.5
2	2-2	22	.15-1
3	5-5	23	0.5
4	1-10	24	1-10
5	2-20	25	3-25
6	4-30	26	6-50
7	5-50	27	10-100
8	10-100		
9	20-200		
	CC Water per min.		Gal. Water per hour
32	6-60	41	6-6
33	10-100	42	2-10
34	20-200	43	3-20
		44	8-40

Model VFB — 4" Scale			
Range No.	Range SCFH Air	Range No.	LPM Air
50	3-3	65	2-4
51	1-10	66	1-10
51	2-20	67	1-20
52	4-40	68	3-30
53	10-100	69	4-40
54	15-150		CC/Min. Water
55	20-200	82	2-30
	SCFM Air		GPH Water
90	3-3	80	.5-12
	CC/Min. Air	83	1-20
60	100-1000	81	6-90
			GPM Water
		85	2-2
		86	5-5

until the first screw has been inserted to expand the boot. Pipe up inlet and discharge using pipe thread sealant tape or pipe thread sealant to insure against leakage.

Surface Mounting on Piping Only: An alternate method of surface mounting is by omitting the mounting screws and supporting the Vis-I-Float® Flowmeter on the connecting piping only. For this method extra long or straight pipe threads should be used so that nuts may be run onto the pipe and later tightened against the back of the panel to retain the unit in proper position. Use the appropriate hole layout information from Figure 1, but omit the small holes.

Mounting on Piping Only Without Panel: For the temporary or laboratory type installation, the panel may be omitted altogether and the flowmeter installed directly in rigid piping. Its light weight permits this without difficulty.

OPERATION

To start system, open the valve slowly to avoid possible damage. Control valves on BV and SSV models are turned clockwise to reduce flow, counter clockwise to increase flow. A nylon insert is provided in the threaded section of the valve stem to give a firm touch to the valve and to prevent change of setting due to vibration.

The performance of low range units used in air or gas applications may be affected by static electricity. Excessive static charge may cause the ball float to behave erratically or provide a false reading. To ensure the proper function of the unit, the application should be designed to minimize or dispel static electricity.

The standard technique for reading a Variable Area Flowmeter is to locate the highest point of greatest diameter on the float, and then align that with the theoretical center of the scale graduation. In the event that the float is not aligned with a grad, an extrapolation of the float location must be made by the operator as to its location between the two closest grads. The following are some sample floats shown with reference to the proper location to read the float.

CAUTION

Do not completely unscrew valve stem unless flowmeter is unpressurized and drained of any liquid. Removal while in service will allow gas or liquid to flow out front of valve body and could result in serious personal injury. For applications involving high pressure and/or toxic gases or fluids, special non-removable valves are available on special order. Contact factory for details.

Variable Area Flowmeters used for gases are typically labeled with the prefix "S" or "N" which represents "Standard" for English units or "Normal" for metric units. Use of this prefix designates that the flowmeter is calibrated to operate at a specific set of conditions, and deviation from those standard conditions will require correction for the calibration to be valid. In practice, the reading taken from the flowmeter scale must be corrected back to standard conditions to be used with the scale units. The correct location to measure the actual pressure and temperature is at the exit of the flowmeter, except under vacuum applications where they should be measured at the flowmeter inlet. The equation to correct for nonstandard operating conditions is as follows:

$$Q_s = Q_a \times \sqrt{\frac{P_a \times T_s}{P_s \times T_a}}$$

Where: Q_a = Actual or Observed Flowmeter Reading
Q_s = Standard Flow Corrected for Pressure and Temperature
P_a = Actual Pressure (14.7 psia + Gage Pressure)
P_s = Standard Pressure (14.7 psia, which is 0 psig)
T_a = Actual Temperature (460 R + Temp °F)
T_s = Standard Temperature (530 R, which is 70°F)

Example: A flowmeter with a scale of 10-100 SCFH Air. The float is sitting at the 60 grad on the flowmeter scale. Actual Pressure is measured at the exit of the meter as 5 psig. Actual Temperature is measured at the exit of the meter as 85°F.

$$Q_s = 60.0 \times \sqrt{\frac{(14.7 + 5) \times 530}{14.7 \times (460 + 85}}$$

Q_s = 68.5 SCFH Air

MAINTENANCE

The only maintenance normally required is occasional cleaning to assure reliable operation and good float visibility.

Disassembly: The flowmeter can be disassembled for cleaning by simply disconnecting the piping, dismounting the unit from the panel and removing the top plug-ball stop. Take out the ball or float by inverting the body and allowing the float to fall into your hand. (Note: It is best to cover the discharge port to avoid losing the float through that opening.) When removing the float guide assembly on VFB models 85 and 86, be careful not to lose the short pieces of plastic tubing on both ends of the guide which serve as float stops.

Cleaning: The flow tube and flowmeter body can best be cleaned with a little pure soap and water. Use of a bottle brush or other soft brush will aid the cleaning. Avoid benzene, acetone, carbon tetrachloride, alkaline detergents, caustic soda, liquid soaps (which may contain chlorinated solvents), etc. and avoid prolonged immersion.

Reassembly: Reinstall the float, remount, connect and place the unit back in service. A little silicone grease or petroleum jelly on the O-rings will help maintain a good seal as well as facilitate assembly. No other special care is required.

For VFB models 85 and 86, first install the lower fitting, next the float guide and float, and finally the upper fitting and plug. Be certain that both ends of the float guide are properly engaged and the float is correctly oriented.

ADDITIONAL INFORMATION

For additional flowmeter application information, conversion curves, factors and other data covering the entire line of Dwyer Instruments, Inc. full-line catalog.

Printed in U.S.A. 7/09 FR# 52-440241-00 Rev.4

DWYER INSTRUMENTS, INC.
P.O. BOX 373 · MICHIGAN CITY, IN 46361, U.S.A.
Phone: 219/879-8000 www.dwyer-inst.com
Fax: 219/872-9057 e-mail: info@dwyer-inst.com

Appendix G-Numerical Models and Validation Video